



First measurement of the cross section for top quark pair production with additional charm jets using dileptonic final states in pp collisions at $\sqrt{s} = 13$ TeV

The CMS Collaboration ^{*}

CERN, Geneva, Switzerland



ARTICLE INFO

Article history:

Received 17 December 2020

Received in revised form 11 June 2021

Accepted 30 July 2021

Available online 4 August 2021

Editor: M. Doser

Keywords:

CMS

Top quark

Dilepton

Charm quark

Charm-tagging

Heavy-flavour

ABSTRACT

The first measurement of the inclusive cross section for top quark pairs ($t\bar{t}$) produced in association with two additional charm jets is presented. The analysis uses the dileptonic final states of $t\bar{t}$ events produced in proton-proton collisions at a centre-of-mass energy of 13 TeV. The data correspond to an integrated luminosity of 41.5 fb^{-1} , recorded by the CMS experiment at the LHC. A new charm jet identification algorithm provides input to a neural network that is trained to distinguish among $t\bar{t}$ events with two additional charm ($t\bar{t}c\bar{c}$), bottom ($t\bar{t}b\bar{b}$), and light-flavour or gluon ($t\bar{t}LL$) jets. By means of a template fitting procedure, the inclusive $t\bar{t}c\bar{c}$, $t\bar{t}b\bar{b}$, and $t\bar{t}LL$ cross sections are simultaneously measured, together with their ratios to the inclusive $t\bar{t}$ + two jets cross section. This provides measurements of the $t\bar{t}c\bar{c}$ and $t\bar{t}b\bar{b}$ cross sections of 10.1 ± 1.2 (stat) ± 1.4 (syst) pb and 4.54 ± 0.35 (stat) ± 0.56 (syst) pb, respectively, in the full phase space. The results are compared and found to be consistent with predictions from two different matrix element generators with next-to-leading order accuracy in quantum chromodynamics, interfaced with a parton shower simulation.

© 2021 The Author(s). Published by Elsevier B.V. This is an open access article under the CC BY license (<http://creativecommons.org/licenses/by/4.0/>). Funded by SCOAP³.

1. Introduction

The modelling of top quark pair ($t\bar{t}$) production in association with jets from the hadronization of bottom (b) or charm (c) quarks, referred to as b jets and c jets, respectively, in proton-proton (pp) collisions at the CERN LHC is challenging. Calculations of the production cross section for top quark pairs with additional pairs of b jets ($t\bar{t}b\bar{b}$) are available at next-to-leading order (NLO) in quantum chromodynamics (QCD) [1–5], but suffer from large uncertainties due to the choice of factorization (μ_F) and renormalization (μ_R) scales. The uncertainties arise from the different energy (or mass) scales in $t\bar{t}b\bar{b}$ production, which range from the large scales associated with the top quark mass (m_t), to the relatively small scales associated with additional jets resulting mostly from gluon splitting into $b\bar{b}$ pairs. To better understand the $t\bar{t}b\bar{b}$ process, the ATLAS and CMS experiments have conducted several measurements in pp collisions at centre-of-mass energies of 7, 8, and 13 TeV [6–13].

The production of a $t\bar{t}$ pair with an additional pair of c jets ($t\bar{t}c\bar{c}$) has received far less attention, both theoretically and experimentally. Whereas the experimental signature of a b jet looks quite different from that of a light-flavour (LF) or gluon jet, the

differences are much less pronounced for c jets. This explains the challenge of simultaneously separating $t\bar{t}c\bar{c}$ and $t\bar{t}b\bar{b}$ events from a large background of $t\bar{t}$ events with additional LF or gluon jets ($t\bar{t}LL$). With the development of a charm jet identification algorithm (“c tagger”) [14], these signatures can now be more efficiently disentangled. We present the first measurement of the inclusive $t\bar{t}c\bar{c}$ cross section and its ratio to the inclusive $t\bar{t}$ + two jets ($t\bar{t}jj$) cross section. A fully consistent treatment of the different additional jet flavours is ensured using a technique that simultaneously extracts the $t\bar{t}c\bar{c}$, $t\bar{t}b\bar{b}$, and $t\bar{t}LL$ cross sections. The measurement is performed in the dileptonic decay channel of the $t\bar{t}$ events using a data sample of pp collisions at a centre-of-mass energy of 13 TeV, collected with the CMS detector in 2017, corresponding to an integrated luminosity of 41.5 fb^{-1} [15]. This data set benefits from the upgrade of the pixel tracking detector [16], which was installed in winter 2016–2017 and which has been shown to significantly improve the performance of heavy-flavour (HF) jet identification [17].

Although the additional b jets in $t\bar{t}b\bar{b}$ events are predominantly produced via gluon splitting into $b\bar{b}$ pairs, they can also originate from the decay of a Higgs boson (H). Previous measurements of Higgs boson production in association with a top quark pair, where the Higgs boson decays into a pair of b quarks ($t\bar{t}H$, $H \rightarrow b\bar{b}$) [18–21], suffer from a nonresonant background of gluon-

^{*} E-mail address: cms-publication-committee-chair@cern.ch.

induced $t\bar{t}b\bar{b}$ events, and to a lesser extent also from $t\bar{t}c\bar{c}$ events due to the misidentification of c jets as b jets. The techniques described here provide a basis for a simultaneous measurement of the $t\bar{t}b\bar{b}$ and $t\bar{t}c\bar{c}$ processes from data that can be adopted in future $t\bar{t}H$ analyses to significantly reduce the uncertainties related to these backgrounds.

2. The CMS detector

The central feature of the CMS apparatus is a superconducting solenoid of 6 m internal diameter, providing a magnetic field of 3.8 T. Within the solenoid volume are a silicon pixel and strip tracker, a lead tungstate crystal electromagnetic calorimeter (ECAL), and a brass and scintillator hadron calorimeter (HCAL), each composed of a barrel and two endcap sections. The silicon tracker measures charged particles within the pseudorapidity range $|\eta| < 2.5$. During the LHC running period when the data used for this analysis were recorded, the silicon tracker consisted of 1856 silicon pixel and 15 148 silicon strip detector modules. For nonisolated particles of $1 < p_T < 10$ GeV and $|\eta| < 2.5$, the track resolutions are typically 1.5% in p_T and 20–75 μm in the transverse impact parameter [22]. Forward calorimeters extend the η coverage provided by the barrel and endcap detectors. Muons are detected in gas-ionization chambers embedded in the steel flux-return yoke outside the solenoid. A more detailed description of the CMS detector, together with a definition of the coordinate system used and the relevant kinematic variables, can be found in Ref. [23].

Events of interest are selected using a two-tiered trigger system [24]. The first level, composed of custom hardware processors, uses information from the calorimeters and muon detectors to select events at a rate of around 100 kHz within a fixed time interval of about 4 μs . The second level, known as the high-level trigger, consists of a farm of processors running a version of the full event reconstruction software optimized for fast processing, and reduces the event rate to around 1 kHz before data storage.

3. Event simulation

Samples of signal and background events are simulated using Monte Carlo (MC) event generators based on a fixed-order perturbative QCD calculation with up to four noncollinear high- p_T partons, supplemented with parton showering (PS) and multiparton interactions. The matrix element (ME) generation of $t\bar{t}$ events is performed with POWHEG (v2) [25–29] at NLO in QCD using the five-flavour scheme, followed by a simulation of the PS using PYTHIA8.230 [30] (referred to as PYTHIA8 in the following), using the CP5 underlying event tune [31] and the NNPDF3.1 [32] parton distribution functions (PDFs). The first additional hard radiation from the $t\bar{t}$ system is included in the NLO ME calculation, whereas higher additional jet multiplicities result from radiation simulated in the PS. A value of $m_t = 172.5$ GeV is used in the event generation and the values of μ_R and μ_F are set to a dynamic scale given by $\sqrt{m_t^2 + p_{T,t}^2}$, where $p_{T,t}$ denotes the transverse momentum of the top quark in the $t\bar{t}$ rest frame. The $t\bar{t}$ cross section is scaled to a theoretical prediction at next-to-next-to-leading order in QCD including resummation of next-to-next-to-leading logarithmic soft-gluon terms, which yields $\sigma_{t\bar{t}} = 832^{+39.9}_{-45.8}$ pb [33]. The results are also compared to those from $t\bar{t}$ production simulated with the MADGRAPH5_AMC@NLO (v2.4.2) [34] ME generator at NLO accuracy using the five-flavour scheme, with FxFx jet matching [35] and including up to two jets in addition to the $t\bar{t}$ system in the NLO ME calculation. No dedicated simulations have been used to model separately $t\bar{t}c\bar{c}$ or $t\bar{t}b\bar{b}$ events, ensuring a consistent treatment between $t\bar{t}c\bar{c}$, $t\bar{t}b\bar{b}$, and $t\bar{t}LL$ events in the inclusive $t\bar{t}$ samples mentioned above.

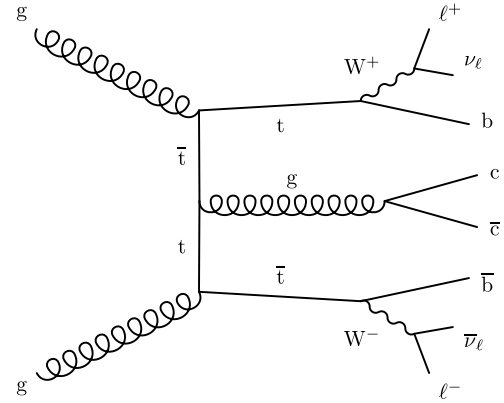


Fig. 1. Example of a Feynman diagram at the lowest order in QCD, describing the dileptonic decay channel of a top quark pair with an additional $c\bar{c}$ pair produced via gluon splitting.

The background processes for this analysis consist mainly of Drell–Yan (DY) and single top quark events, with additional minor contributions from $W + \text{jets}$, diboson, triboson, $t\bar{t}Z$, $t\bar{t}W$, and $t\bar{t}H$ events (collectively referred to as rare backgrounds). For all these samples, the PS is simulated using PYTHIA8. The ME generation of the DY, $W + \text{jets}$, triboson, $t\bar{t}Z$, and $t\bar{t}W$ events is handled using MADGRAPH5_AMC@NLO at leading order in QCD, with MLM jet matching [36]. The $t\bar{t}H$ events are generated at NLO using POWHEG. Single top quark production in the t and s channels are simulated at NLO in the four-flavour scheme using POWHEG and MADGRAPH5_AMC@NLO, respectively, while the tW channel is simulated at NLO with POWHEG in the five-flavour scheme. The diboson samples are simulated at leading order in QCD using PYTHIA8 for both the ME calculations and PS description.

The interactions between particles and the material in the CMS detector are simulated using GEANT4 (v10.02) [37]. The effect of additional pp interactions in the same or nearby beam crossings as the hard-scattering process (pileup) is modelled by adding simulated minimum bias collisions generated in PYTHIA8.

4. Signal definition

A typical Feynman diagram describing the dileptonic $t\bar{t}c\bar{c}$ process is shown in Fig. 1. To provide an unambiguous interpretation of the results, a generator-level definition of the event categories is needed, based on the flavours of the additional jets. The HF jets are identified at the generator level using the procedure of ghost matching [38], where in addition to the reconstructed final-state particles, the generated b and c hadrons are clustered into the jets. However, the modulus of the hadron four-momentum is set to a small number to prevent these generated hadrons from affecting the reconstructed jet momentum and to ensure that only their directional information is retained. Jets that contain both b and c hadrons are labelled as b jets, since the c hadrons most likely originate from a decay of a b hadron. The results of this measurement are reported in terms of the fiducial and full phase spaces.

Fiducial phase space: In the definition of the fiducial phase space, all of the final-state particles (except for the neutrinos) resulting from the decay chain: $pp \rightarrow t\bar{t}jj \rightarrow \ell^+ \nu_\ell b \ell^- \bar{\nu}_\ell \bar{b} j j$ are required to be within the region of the detector in which these objects can be properly reconstructed. The fiducial phase space is therefore defined by the presence of two oppositely charged electrons, muons, or τ leptons (ℓ) at the generator level with $p_T > 25$ GeV and $|\eta| < 2.4$. Each lepton is required to originate from a decay of a W boson, which in turn results from a top quark decay. Particle-level jets are defined by clustering generated final-state particles with a mean lifetime greater than 30 ps, excluding neutrinos, us-

ing the anti- k_T algorithm [39,40] with a distance parameter of 0.4. We demand two particle-level b jets from the top quark decays with $p_T > 20$ GeV and $|\eta| < 2.4$. Besides these two b jets, at least two additional particle-level jets must be present, with the same kinematic requirements imposed. Jets that lie within $\Delta R = \sqrt{(\Delta\eta)^2 + (\Delta\phi)^2} < 0.4$ of either one of the leptons from the W boson decays, where ϕ denotes the azimuthal angle, are excluded. The above requirements define the inclusive $t\bar{t}jj$ signal, which is then subdivided based on the flavour content of the additional particle-level jets (not from the top quark decays) into the following categories:

- $t\bar{t}b\bar{b}$: At least two additional b jets are present, each containing at least one b hadron.
- $t\bar{t}bL$: Only one additional b jet is present, containing at least one b hadron. In addition, at least one additional LF or c jet is present. This category results from $t\bar{t}b\bar{b}$ events in which one of the two additional b jets is outside the acceptance, or two b jets are merged into one.
- $t\bar{t}c\bar{c}$: No additional b jets are present, but at least two additional c jets are found, each containing at least one c hadron.
- $t\bar{t}cL$: No additional b jets are present, and only one additional c jet is found, containing at least one c hadron. In addition, at least one additional LF jet is present. This category results from $t\bar{t}c\bar{c}$ events in which one of the two additional c jets is outside the acceptance, or two c jets are merged into one.
- $t\bar{t}LL$: No additional b or c jets are present, but at least two additional LF jets are within the acceptance.

All other $t\bar{t}$ events that do not fit in any of the above categories, because they do not fulfill the acceptance requirements described in the definition of the fiducial phase space, are labelled as “ $t\bar{t}$ +other”. These could for example be events with semileptonic or fully hadronic $t\bar{t}$ decays that pass the event selection criteria outlined in Section 6, or dileptonic $t\bar{t}$ events for which the leptons or the particle-level jets as described above are not within the fiducial detector volume. These contributions are estimated from the same simulations as those used for the signal events.

Full phase space: The definition of the full phase space comprises dileptonic, semileptonic, and fully hadronic $t\bar{t}$ decays that contain in addition at least two particle-level jets with $p_T > 20$ GeV and $|\eta| < 2.4$. These jets must not originate from the decays of the top quarks or W bosons. There are no requirements imposed on the generator-level leptons or on the particle-level jets that result from the top quark and W boson decays. The measurement in the fiducial phase space is extrapolated to the full phase space by applying an acceptance factor, estimated from simulations, to each signal category based on the additional jet flavours.

The definition of the fiducial phase space is much closer to the reconstructed phase space in which the measurement is performed, and therefore expected to suffer less from theoretical uncertainties that affect the extrapolation from the fiducial to the full phase space. However, the full phase space definition is better suited for comparison with theoretical calculations.

5. Object reconstruction

The global event reconstruction is based on the particle-flow algorithm [41], which aims to reconstruct and identify each individual particle in an event by combining information from the various elements of the CMS detector. The energy of photons is obtained from the ECAL measurement. The energy of electrons is determined from a combination of the electron momentum at the primary interaction vertex as determined by the tracker, the energy of the corresponding ECAL cluster, and the energy sum of all bremsstrahlung photons spatially compatible with originating from

the electron track. The energy of muons is obtained from the curvature of the corresponding track. The energy of charged hadrons is determined from a combination of their momentum measured in the tracker and the matching ECAL and HCAL energy deposits, corrected for zero-suppression effects and for the response function of the calorimeters to hadronic showers. Finally, the energy of neutral hadrons is obtained from the corresponding corrected ECAL and HCAL energies.

For each event, hadronic jets are clustered from these reconstructed particles using the infrared and collinear safe anti- k_T algorithm with a distance parameter of 0.4. Jet momentum is determined as the vectorial sum of all particle momenta in the jet, and is found from simulations to be, on average, within 5 to 10% of the true momentum over the whole p_T spectrum and detector acceptance. Pileup interactions can contribute additional tracks and calorimetric energy depositions, increasing the apparent jet momentum. To mitigate this effect, tracks identified as originating from pileup vertices are discarded and an offset correction is applied to correct for remaining contributions. Jet energy corrections are derived from simulation studies so that the average measured response of jets becomes identical to that of particle-level jets. In situ measurements of the momentum balance in dijet, photon+jets, Z + jets, and multijet events are used to determine any residual differences between the jet energy scale in data and simulations [42], and appropriate corrections are made. Additional selection criteria are applied to each jet to remove jets potentially dominated by instrumental effects or reconstruction failures.

The missing transverse momentum vector \vec{p}_T^{miss} is computed as the negative of the vector sum of the \vec{p}_T of all the particle-flow candidates in an event, and its magnitude is denoted as p_T^{miss} [43]. The \vec{p}_T^{miss} is modified to account for corrections to the energy scale of the reconstructed jets in the event.

The candidate vertex with the largest value of summed physics-object p_T^2 is taken to be the primary pp interaction vertex. The physics objects are the jets and the associated p_T^{miss} .

Jets originating from the hadronization of b and c quarks are identified using the deep combined secondary vertex (DeepCSV) algorithm [14], which uses information on the decay vertices of long-lived mesons and the impact parameters of the charged particle tracks as input to a deep neural network (NN) classifier. For the identification of b jets, a medium working point is chosen, corresponding to a $\approx 70\%$ efficiency for correctly selecting b jets and a misidentification probability for LF (c) jets of $\approx 1(12)\%$, derived from simulated $t\bar{t}$ events. The same algorithm also provides discriminators to distinguish c jets from LF and b jets, which are collectively referred to as c tagging discriminators. The information from the distributions of these observables plays a key role in this analysis, and the calibration of the c tagger is further discussed in Section 8.

6. Event selection

An event selection has been employed to select a subset of events that consists almost exclusively (more than 95% as evaluated from simulations) of dileptonic $t\bar{t}$ events with at least two additional jets. Exactly two reconstructed, oppositely charged leptons (either electrons or muons) are required to be present. This procedure also selects τ leptons that decay into an electron or a muon. The electrons and muons are required to have $p_T > 25$ GeV and $|\eta| < 2.4$, and should be isolated from other objects in the event. At least four jets are required in the event, all of which must be spatially separated from the isolated leptons by imposing $\Delta R(\ell, \text{jet}) > 0.5$. Only jets with $p_T > 30$ GeV and $|\eta| < 2.4$ are considered. An assignment of the jets to the expected partons is made to identify the b jets from top quark decays and jets originating from additional radiation (described in detail in Section 7). The

two jets assigned to the b quarks from the top quark decays are required to be b tagged. Neutrinos from leptonically decaying W bosons are not detected, but instead contribute to the p_T^{miss} , which is required to exceed 30 GeV in events with two electrons (ee) or two muons ($\mu\mu$), in order to reduce contributions from DY events. In events with one electron and one muon ($e\mu$), no requirement is imposed on p_T^{miss} . In order to further reduce the contribution from DY production in ee and $\mu\mu$ events, the invariant mass of the two leptons ($m_{\ell\ell}$) is required to be outside of the Z boson mass window, $m_{\ell\ell} \notin [m_Z - 15, m_Z + 15]$ GeV, with $m_Z = 91.2$ GeV [44]. For all events, it is required that $m_{\ell\ell} > 12$ GeV in order to minimize contributions from low-mass resonances.

7. Matching jets to partons

The distinction among the $t\bar{t}c\bar{c}$, $t\bar{t}b\bar{b}$, and $t\bar{t}L\bar{L}$ categories relies on the correct identification of the additional jets not coming from the decay of the top quarks. Assuming a 100% branching fraction for the decay $t \rightarrow bW$, and focusing on the dileptonic decay channel, two b jets are expected from the top quark decays and at least two additional jets are required through the other event selection criteria. In practice, not all b jets from top quark decays will be reconstructed within the acceptance of the detector and additional jets will also not necessarily pass the reconstruction and selection criteria. In this section, a matching procedure is described to achieve the most accurate correspondence between the final-state jets and the expected partons. This is done by considering all possible permutations of four jets in the collection of jets passing the selection criteria described in Section 6 and training a NN to identify the correct jet-parton assignment.

Whether a given permutation corresponds to a correct jet-parton assignment can be inferred from different quantities, such as the jet kinematic variables, b and c tagging discriminators, and angular separations and invariant masses between pairs of jets (and between jets and leptons). The NN processes, for each event, all possible jet-parton assignments and is trained on the aforementioned observables to give the highest possible score to the correct permutation. For the $t\bar{t}L\bar{L}$, $t\bar{t}c\bar{c}$, and $t\bar{t}cL$ categories, the b and c tagging discriminators dominate the decision made by the NN. For the $t\bar{t}b\bar{b}$ category all four partons have the same flavour, so the correct assignment of the four b jets relies mainly on the angular separations and invariant masses between jets or leptons. The best assignment for the $t\bar{t}bL$ category benefits from a combination of all these observables.

The main objective is to identify additional HF jets in the event. In the assignment of b jets from the $t\bar{t}$ decays, it does not matter which b jet is matched to the decay of the top quark or anti-quark. Any permutation for which these b jets are reversed can still be considered appropriate for this measurement. If at least one additional b or c jet is present, a correct permutation has to identify these as the first or second additional jets. The NN is also trained to choose a permutation in which the first additional jet has a larger b tagging discriminator value than the second additional jet. With these considerations in mind, three output classes are defined. One of the NN outputs denotes the probability for a given permutation to correspond to the correct jet-parton assignment (P^+). Another output class refers to those permutations for which the additional jets are correctly matched, but the b jets from the $t\bar{t}$ decays are reversed as explained above (P^\times). The third output represents all permutations for which the matching is wrong (P^-), meaning that either at least one of the b jets from the $t\bar{t}$ decays is not correctly matched, or an additional HF jet is found but is not identified as either the first or the second additional jet. The best jet-parton assignment is then identified by selecting the permutation with the highest value of:

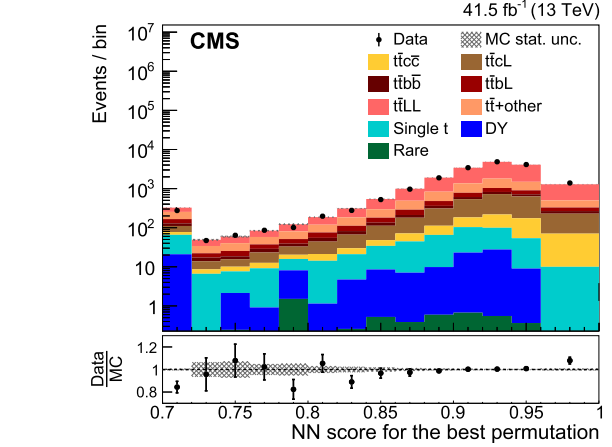


Fig. 2. Comparison between data (points) and simulated predictions (histograms) for the distribution of the NN score for the best permutations of jet-parton assignments found in each event. Underflow is included in the first bin. The distributions are found after the event selections outlined in Section 6, but before fitting the predicted signal yields to the data. The lower panel shows the ratio of the yields in data to those predicted in simulations. The vertical bars represent the statistical uncertainties in data, while the hatched bands show the statistical uncertainty in the simulated predictions.

$$\max\left(\frac{P^+}{P^+ + P^-}, \frac{P^\times}{P^\times + P^-}\right). \quad (1)$$

The NN is trained using the KERAS deep learning library [45], interfaced to TENSORFLOW [46] as a back end. Its architecture is composed of two fully connected hidden layers with 50 neurons each, and with a rectified linear unit activation function. The training is performed using an independent data set of simulated $t\bar{t}$ events that pass all the event selections outlined in Section 6, except for the b tagging requirement. Only events for which the two generator-level b quarks from top quark decays lie within $\Delta R < 0.3$ of a reconstructed b jet are used for the training. These constitute $\approx 76\%$ of the simulated $t\bar{t}$ events with at least two additional jets. Of those, the NN correctly identifies the two additional c (b) jets in 50 (30)% of the cases for $t\bar{t}c\bar{c}$ ($t\bar{t}b\bar{b}$) events. For $t\bar{t}b\bar{b}$ events, the matching is more challenging because the HF tagging information cannot help in separating additional b jets from those originating from top quark decays. A comparison between data and simulations of the NN score for the best permutation in each event is shown in Fig. 2, indicating good agreement between the two.

8. Charm jet identification and calibration

The DeepCSV HF tagging algorithm has a multiclass output structure that predicts the probabilities for each jet to contain a single b hadron ($P(b)$), two b hadrons ($P(bb)$), one or more c hadrons ($P(c)$), or no b or c hadrons ($P(\text{udsg})$). The b tagger used throughout this analysis is constructed from the sum $P(b) + P(bb)$. However, different combinations of output values provide different types of discrimination. Since the displacements of tracks and secondary vertices for c jets are on average smaller than those for b jets and larger than those for LF jets, a charm jet identification algorithm uses a combination of two discriminators. The first is used to distinguish c jets from LF jets (CvsL) and the second separates c jets from b jets (CvsB). The CvsL and CvsB discriminators are defined from the multiclass output structure of the DeepCSV algorithm as:

$$\begin{aligned} \text{CvsL} &= \frac{P(c)}{P(c) + P(\text{udsg})}, \\ \text{CvsB} &= \frac{P(c)}{P(c) + P(b) + P(\text{bb})}. \end{aligned} \quad (2)$$

The c tagging discriminators require calibration with the data, given that these algorithms are trained on simulated events and are therefore prone to mismodelling effects in the input variables. The observed initial discrepancies between the data and the simulated predictions can be as large as 50%, as can be seen from the distributions before calibration in Appendix A. In order to use these c tagger discriminators for the fit of the template distributions (as discussed in Section 9), the shape of the two-dimensional (CvsL, CvsB) distribution is corrected to reproduce the distribution observed in data. To this end, a novel calibration technique is employed that uses three control regions selecting for semileptonic $t\bar{t}$, $W + c$, and $DY + \text{jets}$ events, which are enriched in b , c , and LF jets, respectively [47]. By means of an iterative fit in these three control regions, a set of scale factors for each jet flavour is derived, as a function of both the CvsL and CvsB discriminator values of a given jet. The effectiveness of this calibration for different jet flavours has been validated in the three corresponding control regions outlined above, showing that the calibrated distributions in simulations indeed match those in data within the associated uncertainties. Additionally, the method shows no bias when applied to pseudo-data constructed from simulated events that have artificial scale factors applied to them.

After applying this calibration to the simulated events, the distributions of the CvsL and CvsB discriminators provide a good description of the data, as shown in Fig. 3 for the first (upper row) and second (lower row) additional jet. The uncertainties related to this calibration are further discussed in Section 10.

9. Fit to an event-based neural network discriminator

The extraction of the $t\bar{t}c\bar{c}$, $t\bar{t}b\bar{b}$, and $t\bar{t}LL$ cross sections proceeds by means of a template fit to an observable that can distinguish among the different flavour categories. Since the differentiation relies mainly on the additional-jet flavour, the c tagging discriminators of the first and second additional jets provide a natural choice for separating the different signals. The CvsL discriminator distinguishes the $t\bar{t}c\bar{c}$ and $t\bar{t}b\bar{b}$ from the $t\bar{t}LL$ events, whereas the CvsB discriminator provides additional information that can be used to distinguish between the $t\bar{t}c\bar{c}$ and $t\bar{t}b\bar{b}$ events. The flavour tagging information for the second additional jet allows the $t\bar{t}cL$ and $t\bar{t}bL$ processes to be identified. Additional information is extracted from two kinematic variables. The first is the angular separation ΔR between the two additional jets. In the $t\bar{t}c\bar{c}$ and $t\bar{t}b\bar{b}$ processes, the additional jets arise predominantly from gluon splitting into $c\bar{c}$ and $b\bar{b}$ pairs, respectively, and are therefore expected to be more collimated. The second is the NN score for the best permutation (shown in Fig. 2), which is expected to be larger on average for $t\bar{t}LL$ events because the additional jets are well distinguished from the b jets from top quark decays. This observable indirectly incorporates information on the event kinematic features through its input variables.

Using the six aforementioned observables, a NN is trained. Given the relatively small number of inputs, an architecture for the NN is chosen with one hidden layer that comprises 30 neurons with a rectified linear unit activation function. This NN predicts output probabilities for five output classes: $P(t\bar{t}c\bar{c})$, $P(t\bar{t}cL)$, $P(t\bar{t}b\bar{b})$, $P(t\bar{t}bL)$, and $P(t\bar{t}LL)$. To obtain the distributions that are used in the fit, these probabilities are projected onto a two-dimensional phase space spanned by two derived discriminators:

Table 1

Selection efficiencies and acceptance factors for events in different signal categories. The values are obtained from simulated $t\bar{t}$ events.

| Event category | $t\bar{t}b\bar{b}$ | $t\bar{t}bL$ | $t\bar{t}c\bar{c}$ | $t\bar{t}cL$ | $t\bar{t}LL$ |
|------------------------------|--------------------|--------------|--------------------|--------------|--------------|
| Efficiency ϵ (%) | 12.0 | 8.5 | 6.8 | 5.6 | 4.5 |
| Acceptance \mathcal{A} (%) | 2.9 | 2.5 | 2.0 | 2.0 | 2.3 |

$$\begin{aligned} \Delta_b^c &= \frac{P(t\bar{t}c\bar{c})}{P(t\bar{t}c\bar{c}) + P(t\bar{t}b\bar{b})}, \\ \Delta_L^c &= \frac{P(t\bar{t}c\bar{c})}{P(t\bar{t}c\bar{c}) + P(t\bar{t}LL)}. \end{aligned} \quad (3)$$

These discriminators can be interpreted as topology-specific c tagger discriminators that augment the information on the jet flavour of the two additional jets with additional event kinematic features to optimally distinguish different signal categories. The two-dimensional distributions of these discriminators, normalized to unit area, are shown in Fig. 4 for simulated dileptonic $t\bar{t}$ events. The different signal categories occupy different parts of this phase space, demonstrating that a fit of templates derived from these distributions to the data can be used to extract the $t\bar{t}c\bar{c}$, $t\bar{t}b\bar{b}$, and $t\bar{t}LL$ cross sections. It can be seen that the lower right corner of this phase space is almost exclusively populated with $t\bar{t}b\bar{b}$ events, whereas the upper right corner is dominated by $t\bar{t}c\bar{c}$ events.

Templates are constructed separately for each dilepton channel (ee , $\mu\mu$, and $e\mu$) and are fitted simultaneously to data by means of a binned maximum likelihood fit assuming Poisson statistics. The negative logarithm of the likelihood is minimized using the ‘‘Combine’’ framework developed for the combined Higgs boson measurements performed by ATLAS and CMS [48,49]. Uncertainties are included as nuisance parameters in the definition of the likelihood.

A first fit is performed to extract the absolute cross section (σ) of the $t\bar{t}c\bar{c}$, $t\bar{t}b\bar{b}$, and $t\bar{t}LL$ events in the fiducial phase space, where the expected yield in each bin is parametrized using the function:

$$\begin{aligned} F_i(\sigma_{t\bar{t}c\bar{c}}, \sigma_{t\bar{t}b\bar{b}}, \sigma_{t\bar{t}LL}) = & \\ \mathcal{L}^{\text{int}} \left\{ \sigma_{t\bar{t}c\bar{c}} \epsilon_{t\bar{t}c\bar{c}} \left(f_{t\bar{t}c\bar{c},i}^{\text{norm}} + \frac{N_{t\bar{t}c\bar{c}}^{\text{MC}}}{N_{t\bar{t}c\bar{c}}^{\text{MC}}} f_{t\bar{t}cL,i}^{\text{norm}} \right) \right. & \\ + \sigma_{t\bar{t}b\bar{b}} \epsilon_{t\bar{t}b\bar{b}} \left(f_{t\bar{t}b\bar{b},i}^{\text{norm}} + \frac{N_{t\bar{t}bL}^{\text{MC}}}{N_{t\bar{t}b\bar{b}}^{\text{MC}}} f_{t\bar{t}bL,i}^{\text{norm}} \right) & \\ + \sigma_{t\bar{t}LL} \epsilon_{t\bar{t}LL} \left(f_{t\bar{t}LL,i}^{\text{norm}} + \frac{N_{t\bar{t}+other}^{\text{MC}}}{N_{t\bar{t}LL}^{\text{MC}}} f_{t\bar{t}+other,i}^{\text{norm}} \right) \Big\} & \\ + \mathcal{L}^{\text{int}} \sigma_{\text{bkg}} f_{\text{bkg},i}^{\text{norm}}. & \end{aligned} \quad (4)$$

Here, \mathcal{L}^{int} denotes the total integrated luminosity and f_i^{norm} represents a given bin (with index i) of the simulated two-dimensional template, normalized to unit area. The measurements in the reconstructed phase space are corrected to the fiducial phase space through an efficiency (ϵ). To extract the result in the full phase space, an additional acceptance factor, \mathcal{A} , is applied to the extracted fiducial cross section to account for the difference in acceptance between the fiducial and full phase spaces. The efficiency and acceptance factors are summarized in Table 1, and are calculated from simulations. The largest contribution to the acceptance can be attributed to the extrapolation from the dileptonic to the fully inclusive decays of the $t\bar{t}$ pairs. The remaining contributions are due to changes in kinematic requirements on the generator-level objects. As discussed in Section 4, the $t\bar{t}cL$ and $t\bar{t}bL$ categories result from $t\bar{t}c\bar{c}$ and $t\bar{t}b\bar{b}$ events, respectively, where one of the additional HF jets is outside the acceptance or both are merged

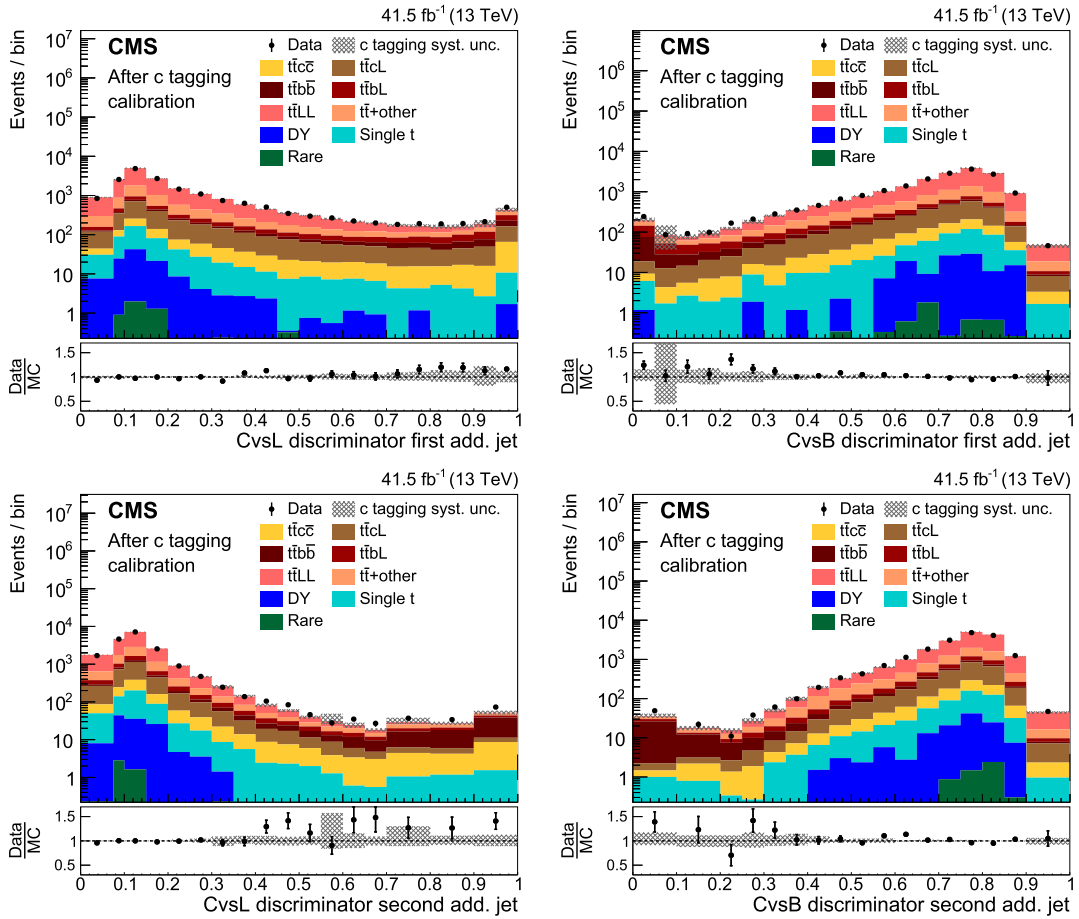


Fig. 3. Comparison between data (points) and simulated predictions (histograms) for the CvsL (left column) and CvsB (right column) c tagging discriminator distributions of the first (upper row) and second (lower row) additional jet after applying the c tagging calibration. The distributions are found after the event selections outlined in Section 6, but before fitting the predicted signal yields to the data. The lower panels show the ratio of the yields in data to those predicted in simulations. The vertical bars represent the statistical uncertainties in data, while the hatched bands show the systematic uncertainty from the c tagging calibration only.

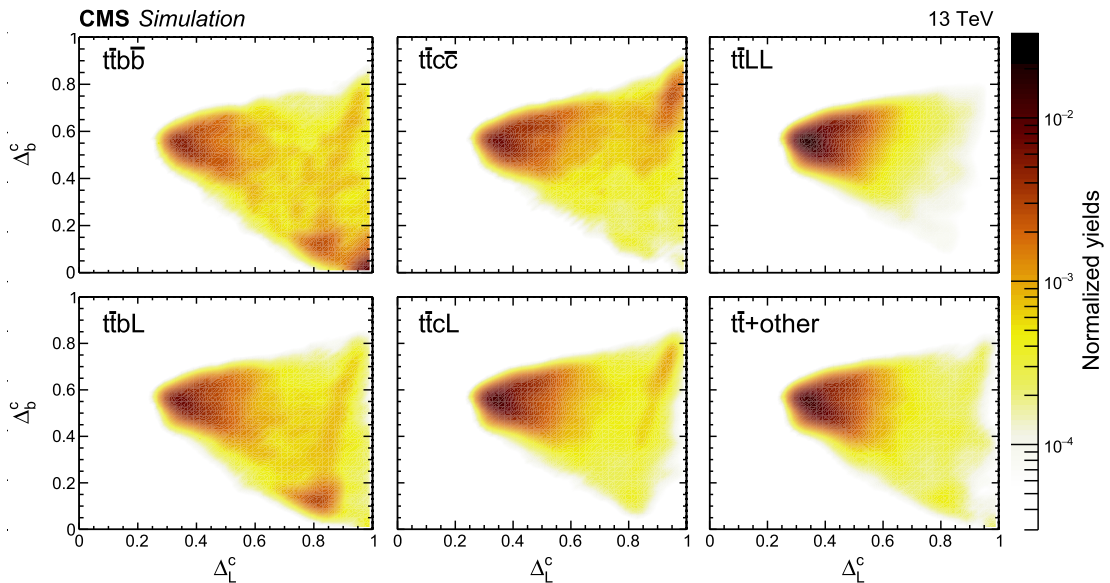


Fig. 4. Normalized two-dimensional distributions of Δ_b^c vs. Δ_L^c in simulated dileptonic $t\bar{t}$ events, for each of the event categories outlined in Section 4. The colour scale on the right shows the normalized event yields.

into one jet. Therefore, these components are scaled with the same factors as the $t\bar{t}c\bar{c}$ and $t\bar{t}b\bar{b}$ templates, respectively, such that the relative yield of $t\bar{t}cL$ ($t\bar{t}bL$) with respect to $t\bar{t}c\bar{c}$ ($t\bar{t}b\bar{b}$) events is fixed to that predicted in the simulations. The predicted yields from the simulations are denoted by N_k^{MC} , where k denotes the signal process. The $t\bar{t}$ +other component is scaled with the same factor as the $t\bar{t}LL$ component, motivated by their similar LF content. Uncertainties in the ratios of simulated yields are taken into account in the fit. The background processes are summed together into one template and their yield is fixed to the predictions from simulations, with uncertainties taken into account as discussed in Section 10. The sum of the cross sections for the background processes (obtained from simulations) is denoted as σ_{bkg} .

A second binned maximum likelihood fit is performed assuming Poisson statistics to extract the ratios of the $t\bar{t}c\bar{c}$ and $t\bar{t}b\bar{b}$ cross sections to the overall inclusive $t\bar{t}jj$ cross section (denoted R_c and R_b , respectively) in the fiducial phase space, with the expected yield in bin i calculated using the function:

$$F_i(\sigma_{t\bar{t}jj}, R_c, R_b) = \mathcal{L}^{\text{int}} \sigma_{t\bar{t}jj} \left\{ R_c \epsilon_{t\bar{t}c\bar{c}} \left(f_{t\bar{t}c\bar{c},i}^{\text{norm}} + \frac{N_{t\bar{t}cL}^{MC}}{N_{t\bar{t}c\bar{c}}^{MC}} f_{t\bar{t}cL,i}^{\text{norm}} \right) + R_b \epsilon_{t\bar{t}b\bar{b}} \left(f_{t\bar{t}b\bar{b},i}^{\text{norm}} + \frac{N_{t\bar{t}bL}^{MC}}{N_{t\bar{t}b\bar{b}}^{MC}} f_{t\bar{t}bL,i}^{\text{norm}} \right) + (1 - R_c - R_{cL} - R_b - R_{bL}) \epsilon_{t\bar{t}LL} \left(f_{t\bar{t}LL,i}^{\text{norm}} + \frac{N_{t\bar{t}+other}^{MC}}{N_{t\bar{t}LL}^{MC}} f_{t\bar{t}+other,i}^{\text{norm}} \right) \right\} + \mathcal{L}^{\text{int}} \sigma_{bkg} f_{bkg,i}^{\text{norm}},$$

with

$$\begin{cases} R_{cL} = R_c \left(\frac{N_{t\bar{t}cL}^{MC} \epsilon_{t\bar{t}c\bar{c}}}{N_{t\bar{t}c\bar{c}}^{MC} \epsilon_{t\bar{t}cL}} \right), \\ R_{bL} = R_b \left(\frac{N_{t\bar{t}bL}^{MC} \epsilon_{t\bar{t}b\bar{b}}}{N_{t\bar{t}b\bar{b}}^{MC} \epsilon_{t\bar{t}bL}} \right). \end{cases} \quad (6)$$

The parameters R_{cL} and R_{bL} are used to denote, respectively, the ratios of the $t\bar{t}cL$ and $t\bar{t}bL$ cross sections to the inclusive $t\bar{t}jj$ cross section, and are defined as a function of R_c and R_b in Eq. (6).

10. Systematic uncertainties

This section summarizes the systematic uncertainties related to the extraction of the $t\bar{t}c\bar{c}$, $t\bar{t}b\bar{b}$, and $t\bar{t}LL$ cross sections (and the ratios R_c and R_b), as well as corrections applied to the simulated events to account for differences with respect to data. Systematic uncertainties are treated as nuisance parameters in the template fit to data that can affect both the shapes of the templates and the yields of the signal and background processes. A smoothing procedure [50] is applied to the templates that describe the uncertainty variations affecting the template shape. The sources of systematic uncertainties are subdivided into experimental and theoretical components and are discussed below.

Experimental uncertainties: These uncertainties affect both the shape and normalization of the templates. The jet energy resolution is known to be worse in data than in simulations, and a corresponding additional smearing is applied to the simulated jet energies [42]. Systematic uncertainties are estimated by varying the smearing of the jet energy within its uncertainties in the calculation of the cross sections. Similarly, we take into account corrections and uncertainties from observed differences in the jet

energy scale. These corrections are evaluated and applied in different regions of jet p_T and $|\eta|$. Observed differences in electron and muon identification, isolation, reconstruction, and trigger efficiencies between data and simulations are taken into account through p_T - and η -dependent scale factors, with the corresponding uncertainties accounted for. The distribution of the number of pileup collisions in simulated events is reweighted to match the distribution observed in data, using an inelastic pp cross section of 69.2 mb [51]. An uncertainty related to this correction is applied by varying this inelastic cross section by $\pm 4.6\%$. An uncertainty of 2.3% [15] in the total integrated luminosity is also taken into account. The scale factors extracted from the c tagging calibration are applied to the simulated events, and corresponding uncertainties are considered. Uncertainties related to this calibration are found to be dominated by the choice of μ_R and μ_F in the $W + c$ and $DY + jets$ control regions, affecting scale factors for c and LF jets, respectively, and by PS uncertainties in semileptonic $t\bar{t}$ events that affect scale factors for b jets, together with a significant contribution from statistical uncertainties for all jet flavours. Most of the theoretical and experimental sources of uncertainty are in common between the control regions in which the c tagging calibration is derived and the $t\bar{t}$ dileptonic signal region considered in this analysis. In such cases, the common uncertainties are considered fully correlated and evaluated simultaneously.

Theoretical uncertainties: In the ME calculation, the choice of μ_R and μ_F can have an impact on the kinematic distributions of the final-state objects. Uncertainties in these scales are taken into account by rescaling μ_F and μ_R up or down by a factor of two at the ME level [52,53]. The choice was made not to include the difference between PYTHIA and alternative PS simulations as a systematic uncertainty in this analysis. Instead a variety of parameters in PYTHIA, sensitive to the PS and hadronization, are consistently varied to assess the uncertainty in an unambiguous way. In the PS, the uncertainty in the value of the strong coupling constant (α_S) evaluated at m_Z is taken into account by varying the renormalization scale of QCD emissions in the initial- and final-state radiation up and down by a factor of two. Similarly, uncertainties in the momentum transfer from b quarks to b hadrons (b fragmentation) in the PS have been included. The b fragmentation in PYTHIA is parametrized using a Bowler–Lund model [54–56], with uncertainties calculated by tuning the internal parameters of this model to measurements from the ALEPH [57], DELPHI [58], OPAL [59] and SLD [60] experiments. In practice, it was found that this parametrization can be varied within its uncertainties by a reweighting at the generator level of the so-called “transfer function”, $x_b = p_T(b \text{ hadron})/p_T(b \text{ jet})$. No such detailed assessment of the c fragmentation uncertainties has yet been performed, but a similar level of variation is observed when comparing the available experimental measurements [61] with the default PYTHIA tune used in this analysis [62]. We verified that variations of the c jet transfer function ($x_c = p_T(c \text{ hadron})/p_T(c \text{ jet})$) induce similar variations of the c jet p_T and c tagging discriminator distributions as the analogous variations in b fragmentation for b jets, and found that these effects are comfortably covered by an uncertainty a factor of two larger than that for b fragmentation. This uncertainty is modelled as an uncertainty in the $t\bar{t}c\bar{c}$ and $t\bar{t}cL$ yields in the fit in the fiducial phase space, and an additional uncertainty in the acceptance correction from the full to the fiducial phase space. Uncertainties associated with the PDF, as well as with the value of α_S in the PDF of the proton are considered, following the PDF4LHC prescription [63]. For all of the aforementioned theoretical sources of uncertainty (except for the c fragmentation uncertainty), the effects of these variations on the shape of the fitted templates are taken into account in the fit, whereas their impact on the signal yields is considered as an uncertainty in the theoretical prediction to which the measurement is compared in Section 11. The resid-

Table 2

Sources of theoretical uncertainties in the acceptance, used to extrapolate the results from the fiducial to the full phase space, for different signal categories, together with their individual impact in percent. The last row of the table quotes the total relative uncertainty in the acceptance, calculated by adding in quadrature the effects from individual sources. A dash indicates that the uncertainty is not applicable for that signal category.

| Sources | Uncertainty in the acceptance (%) | | | | |
|---------------------|-----------------------------------|--------------|--------------------|--------------|--------------|
| | $t\bar{t}c\bar{c}$ | $t\bar{t}cL$ | $t\bar{t}b\bar{b}$ | $t\bar{t}bL$ | $t\bar{t}LL$ |
| μ_R and μ_F | 1.0 | 0.8 | 0.4 | 0.6 | 0.5 |
| PS scale | 1.6 | 1.6 | 1.2 | 1.4 | 1.5 |
| PDF | 0.6 | 0.8 | 1.2 | 1.2 | 0.9 |
| Underlying event | 1.0 | 1.2 | 1.8 | 1.1 | 0.3 |
| ME-PS matching | 2.1 | 2.3 | 1.0 | 2.5 | 1.7 |
| b fragmentation | 2.2 | 2.0 | 4.2 | 2.6 | 2.3 |
| c fragmentation | 4.5 | 2.0 | – | – | – |
| Total | 5.9 | 4.3 | 5.0 | 4.2 | 3.4 |

ual theoretical uncertainty that enters the measured cross sections through the ϵ_i terms in Eqs. (4) and (5) is accounted for by a separate theoretical uncertainty in the efficiency. The experimental uncertainties in the efficiency are already taken into account through the uncertainties in the normalization of the templates. The matching between the ME and PS is governed by a parameter called h_{damp} . The value of this parameter is varied according to $h_{\text{damp}} = \left(1.379^{+0.926}_{-0.505}\right) m_t$ [31] in a separate simulation. Since the size of this simulated data set is insufficient to reliably estimate the effect on the shapes of the templates, this uncertainty is conservatively estimated through its effect on the overall yield. The remnants of the pp collisions that do not take part in the hard scattering are referred to as the underlying event. Their kinematic distributions are tuned in the generators to match those observed in the data [31]. The resulting parametrization of the CP5 tune, used in this analysis, is varied within its uncertainties in separate simulations. Here too the effect of the uncertainty in the overall yield, rather than in the template shapes, is propagated to the measured cross sections. The effects of the theoretical uncertainties listed above on the fixed ratios of $t\bar{t}bL$ to $t\bar{t}b\bar{b}$, $t\bar{t}cL$ to $t\bar{t}c\bar{c}$, and $t\bar{t}$ -other to $t\bar{t}LL$ yields, taken from simulations in Eqs. (4) and (5), are also included in the fit. An uncertainty of 25% is assigned to the total cross section of all background processes, based on the precision of recent measurements of the dominant background processes [64,65]. The statistical uncertainty due to the finite size of the simulated samples is taken into account in the fit. In extrapolating the results from the fiducial to the full phase space, some of these theoretical uncertainties also affect the acceptance for the different signal categories. The individual and combined impacts of different sources of uncertainty in the acceptance are summarized in Table 2.

The individual impacts from each source of uncertainty in the cross sections (and ratios) for the fiducial phase space after the fit are summarized in Table 3. The fitted nuisance parameters do not deviate significantly from their initial values and are not significantly constrained. No strong correlations between any of the nuisance parameters and the fitted cross sections or ratios are observed. The dominant systematic uncertainties are related to the c tagging calibration, followed by jet energy scale and fragmentation uncertainties, as well as uncertainties related to the matching between ME and PS, and the choice of μ_R and μ_F scales in the ME calculation.

11. Results

The binning of the two-dimensional Δ_L^c vs. Δ_b^c distribution is chosen to be:

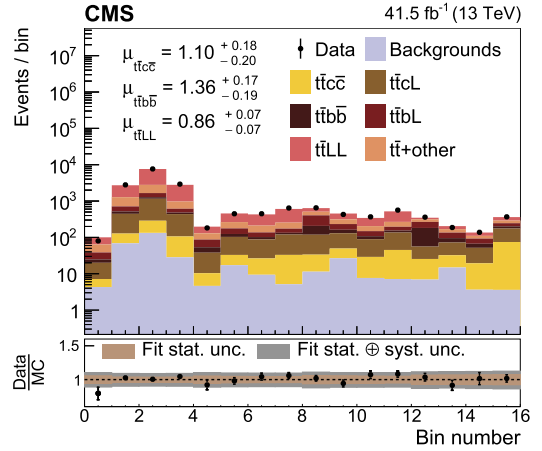


Fig. 5. A one-dimensional representation of the two-dimensional Δ_L^c vs. Δ_b^c distributions, in the simulations (histograms) and in data (points), after normalizing the simulated templates according to the fitted cross sections. The lower panel shows the ratio of the yields in data to those predicted in the simulations. The brown and grey uncertainty bands denote, respectively, the statistical and total uncertainties from the fit. The factors (μ) by which the templates of the different processes (using the POWHEG ME generator) are scaled, are also displayed, together with their combined statistical and systematic uncertainties.

$$\Delta_L^c \otimes \Delta_b^c :$$

$$[0, 0.55, 0.65, 0.85, 1.0] \otimes [0, 0.35, 0.5, 0.6, 1.0]. \quad (7)$$

This gives a total of 16 bins with varying compositions of signal categories. From these 16 bins, a one-dimensional histogram is created in which the first four bins correspond to the first bin in Δ_b^c , with increasing values of Δ_L^c , and then analogously for the remainder of the bins. This histogram is shown in Fig. 5 after normalizing the simulated templates according to the fitted cross sections. The factors by which the templates of the $t\bar{t}c\bar{c}$, $t\bar{t}b\bar{b}$, and $t\bar{t}LL$ processes (using the POWHEG ME generator) are scaled to match the data are denoted $\mu_{t\bar{t}c\bar{c}}$, $\mu_{t\bar{t}b\bar{b}}$, and $\mu_{t\bar{t}LL}$, respectively. Their measured values from the fit are displayed in the top panel of Fig. 5, together with their combined statistical and systematic uncertainties. An improved agreement between data and simulated predictions is also observed for the c tagging discriminators of the first and second additional jets after normalizing the simulated templates according to the fitted cross sections. This is demonstrated in Appendix B and can be directly compared to the agreement before the fit in Fig. 3.

The measured cross sections in the fiducial and full phase spaces, together with their statistical and systematic uncertainties, are summarized in Table 4 and compared to predictions using the POWHEG and MADGRAPH5_AMC@NLO ME generators. Uncertainties in the measured values of the cross sections and ratios are determined from the points where the decrease in the logarithm of the profiled likelihood from the best-fit value intersects with 0.5. The inclusive $t\bar{t}c\bar{c}$ cross section and the ratio R_c are measured here for the first time. They are in agreement with the predictions from both ME generators, within the uncertainties.

In addition, two-dimensional likelihood scans are performed over different combinations of cross sections or ratios. These are shown in Fig. 6 for the measurements in the fiducial phase space. The 68 and 95% confidence level contours are shown, along with the predictions from the POWHEG and MADGRAPH5_AMC@NLO ME generators. Agreement is observed at the level of one to two standard deviations between the measured values and simulated predictions for the $t\bar{t}c\bar{c}$, $t\bar{t}b\bar{b}$, and $t\bar{t}LL$ processes. The most significant tension is observed in the ratio R_b , at the level of 2.5 standard deviations. Results for $\sigma_{t\bar{t}b\bar{b}}$ and R_b are consistent with previous measurements targeting specifically this signature [6–13] and show the

same tendency to be slightly above the predictions from simulations.

12. Summary

The production of a top quark pair ($t\bar{t}$) in association with additional bottom or charm jets at the LHC provides challenges both in the theoretical modelling and experimental measurement of this process. Whereas $t\bar{t}$ production with two additional bottom jets ($t\bar{t}b\bar{b}$) has been measured by the ATLAS and CMS Collaborations at different centre-of-mass energies [6–13], this analysis presents the first measurement of the cross section for $t\bar{t}$ production with two additional charm jets ($t\bar{t}c\bar{c}$). The analysis is conducted using data from proton-proton collisions recorded by the CMS experiment at a centre-of-mass energy of 13 TeV, corresponding to an integrated luminosity of 41.5 fb^{-1} . The measurement is performed in the dileptonic channel of the $t\bar{t}$ decays and relies on the use of recently developed charm jet identification algorithms (c tagging). A template fitting method is used, based on the outputs of

a neural network classifier trained to identify the signal categories defined by the flavour of the additional jets. This allows the simultaneous extraction of the cross section for the $t\bar{t}c\bar{c}$, $t\bar{t}b\bar{b}$, and $t\bar{t}$ with two additional light-flavour or gluon jets ($t\bar{t}LL$) processes. A novel multidimensional calibration of the shape of the c tagging discriminator distributions is employed, such that this information can be reliably used in the neural network classifier.

The $t\bar{t}c\bar{c}$ cross section is measured for the first time to be $0.207 \pm 0.025 \text{ (stat)} \pm 0.027 \text{ (syst)} \text{ pb}$ in the fiducial phase space (matching closely the sensitive region of the detector) and $10.1 \pm 1.2 \text{ (stat)} \pm 1.4 \text{ (syst)} \text{ pb}$ in the full phase space. The ratio of the $t\bar{t}c\bar{c}$ to the inclusive $t\bar{t}$ + two jets cross sections is found to be $(3.01 \pm 0.34 \text{ (stat)} \pm 0.31 \text{ (syst)})\%$ in the fiducial phase space and $(3.36 \pm 0.38 \text{ (stat)} \pm 0.34 \text{ (syst)})\%$ in the full phase space. These results are compared with predictions from two different matrix element generators with next-to-leading order accuracy in quantum chromodynamics, in which an inclusive description of the $t\bar{t}$ process, with up to two additional radiated hard gluons at the

Table 3

Classes of systematic uncertainties in the measured parameters and their individual impact in percent after the fit for the fiducial phase space. The upper (lower) rows of the table list uncertainties related to the experimental conditions (theoretical modelling). For classes describing contributions from multiple nuisance parameters, the quoted numbers are obtained by adding the impacts from individual sources within that class in quadrature. The last row gives the overall systematic uncertainty in each quantity, which results from the nuisance parameter variations in the fit and is not the quadrature sum of the individual components.

| Sources | Systematic uncertainty (%) | | | | |
|---|-----------------------------------|-----------------------------------|-----------------------------|--------------|--------------|
| | $\Delta\sigma_{t\bar{t}c\bar{c}}$ | $\Delta\sigma_{t\bar{t}b\bar{b}}$ | $\Delta\sigma_{t\bar{t}LL}$ | ΔR_c | ΔR_b |
| Jet energy scale | 4.0 | 3.2 | 4.7 | 2.8 | 2.1 |
| Jet energy resolution | 2.3 | 1.0 | 0.9 | 2.5 | 1.3 |
| c tagging calibration | 7.0 | 3.2 | 2.5 | 7.3 | 3.5 |
| Lepton identification and isolation | 0.8 | 1.0 | 1.3 | 0.6 | 0.3 |
| Trigger | 2.0 | 2.0 | 2.0 | < 0.1 | < 0.1 |
| Pileup | 0.3 | 0.2 | 0.3 | 0.5 | < 0.1 |
| Total integrated luminosity | 2.3 | 2.4 | 2.3 | < 0.1 | < 0.1 |
| μ_R and μ_F scales in ME | 3.3 | 6.2 | 2.1 | 3.8 | 6.8 |
| PS scale | 0.4 | 1.6 | 0.3 | 0.5 | 1.6 |
| PDF | 0.3 | 0.1 | 0.1 | 0.2 | 0.1 |
| ME-PS matching | 7.1 | 5.7 | 3.5 | 2.6 | 1.5 |
| Underlying event | 1.9 | 2.3 | 1.1 | 0.5 | 0.9 |
| b fragmentation | 0.4 | 1.9 | 0.8 | 0.3 | 2.4 |
| c fragmentation | 4.6 | < 0.1 | < 0.1 | 3.9 | 0.7 |
| $t\bar{t}b(L)/t\bar{t}b\bar{b}(c\bar{c})$ and $t\bar{t}$ +other/ $t\bar{t}LL$ | 2.4 | 1.8 | 1.1 | 1.8 | 1.5 |
| Efficiency (theoretical) | 2.4 | 2.1 | 2.0 | < 0.1 | < 0.1 |
| Simulated sample size | 3.2 | 2.6 | 1.1 | 3.1 | 2.5 |
| Background normalization | 0.5 | 0.7 | 0.6 | 0.1 | 0.1 |
| Total | 13.7 | 11.4 | 8.2 | 10.9 | 9.2 |

Table 4

Measured parameter values in the fiducial (upper rows) and full (lower rows) phase spaces with their statistical and systematic uncertainties listed in that order. The last two columns display the expectations from the simulated $t\bar{t}$ samples using the POWHEG or MADGRAPH5_AMC@NLO ME generators. The uncertainties quoted for these predictions include the contributions from the theoretical uncertainties listed in the lower rows of Table 3, as well as the uncertainty in the $t\bar{t}$ cross section.

| | Result | POWHEG | MADGRAPH5_AMC@NLO |
|----------------------------------|-----------------------------|-------------------|-------------------|
| Fiducial phase space | | | |
| $\sigma_{t\bar{t}c\bar{c}}$ [pb] | $0.207 \pm 0.025 \pm 0.027$ | 0.187 ± 0.038 | 0.189 ± 0.032 |
| $\sigma_{t\bar{t}b\bar{b}}$ [pb] | $0.132 \pm 0.010 \pm 0.015$ | 0.097 ± 0.021 | 0.101 ± 0.023 |
| $\sigma_{t\bar{t}LL}$ [pb] | $5.15 \pm 0.12 \pm 0.41$ | 5.95 ± 1.02 | 6.32 ± 0.94 |
| R_c [%] | $3.01 \pm 0.34 \pm 0.31$ | 2.53 ± 0.18 | 2.43 ± 0.17 |
| R_b [%] | $1.93 \pm 0.15 \pm 0.18$ | 1.31 ± 0.12 | 1.30 ± 0.16 |
| Full phase space | | | |
| $\sigma_{t\bar{t}c\bar{c}}$ [pb] | $10.1 \pm 1.2 \pm 1.4$ | 9.1 ± 1.8 | 8.9 ± 1.5 |
| $\sigma_{t\bar{t}b\bar{b}}$ [pb] | $4.54 \pm 0.35 \pm 0.56$ | 3.34 ± 0.72 | 3.39 ± 0.66 |
| $\sigma_{t\bar{t}LL}$ [pb] | $220 \pm 5 \pm 19$ | 255 ± 43 | 261 ± 37 |
| R_c [%] | $3.36 \pm 0.38 \pm 0.34$ | 2.81 ± 0.20 | 2.72 ± 0.19 |
| R_b [%] | $1.51 \pm 0.11 \pm 0.16$ | 1.03 ± 0.08 | 1.03 ± 0.09 |

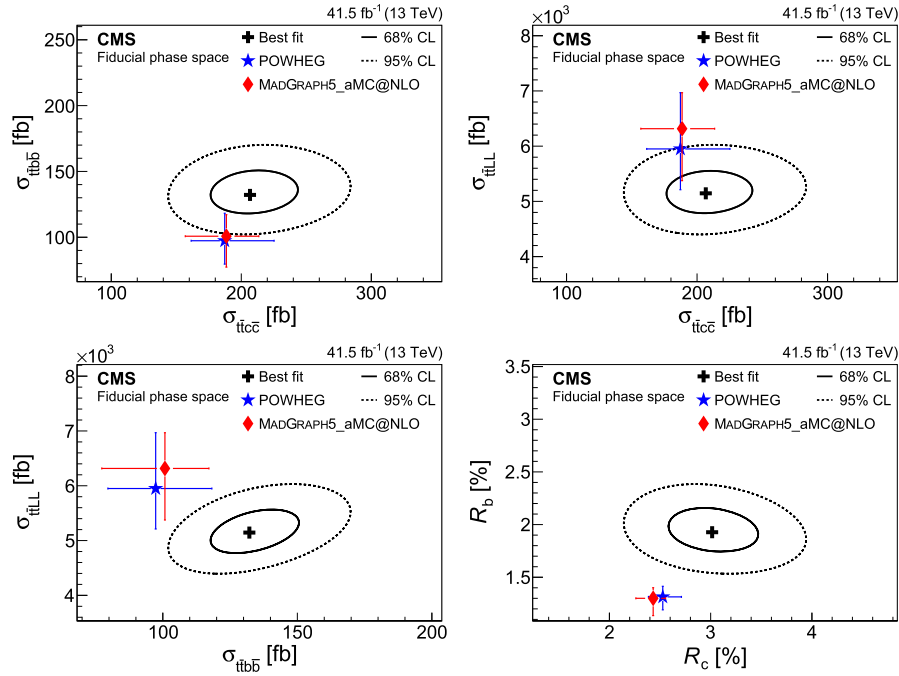


Fig. 6. Results of the two-dimensional likelihood scans for several combinations of the parameters of interest in the fiducial phase space. The best-fit value (black cross) with the corresponding 68% (full) and 95% (dashed) confidence level (CL) contours are shown, compared to the theoretical predictions using either the POWHEG (blue star) or MADGRAPH5_aMC@NLO (red diamond) ME generators. Uncertainties in the theoretical predictions are displayed by the horizontal and vertical bars on the markers.

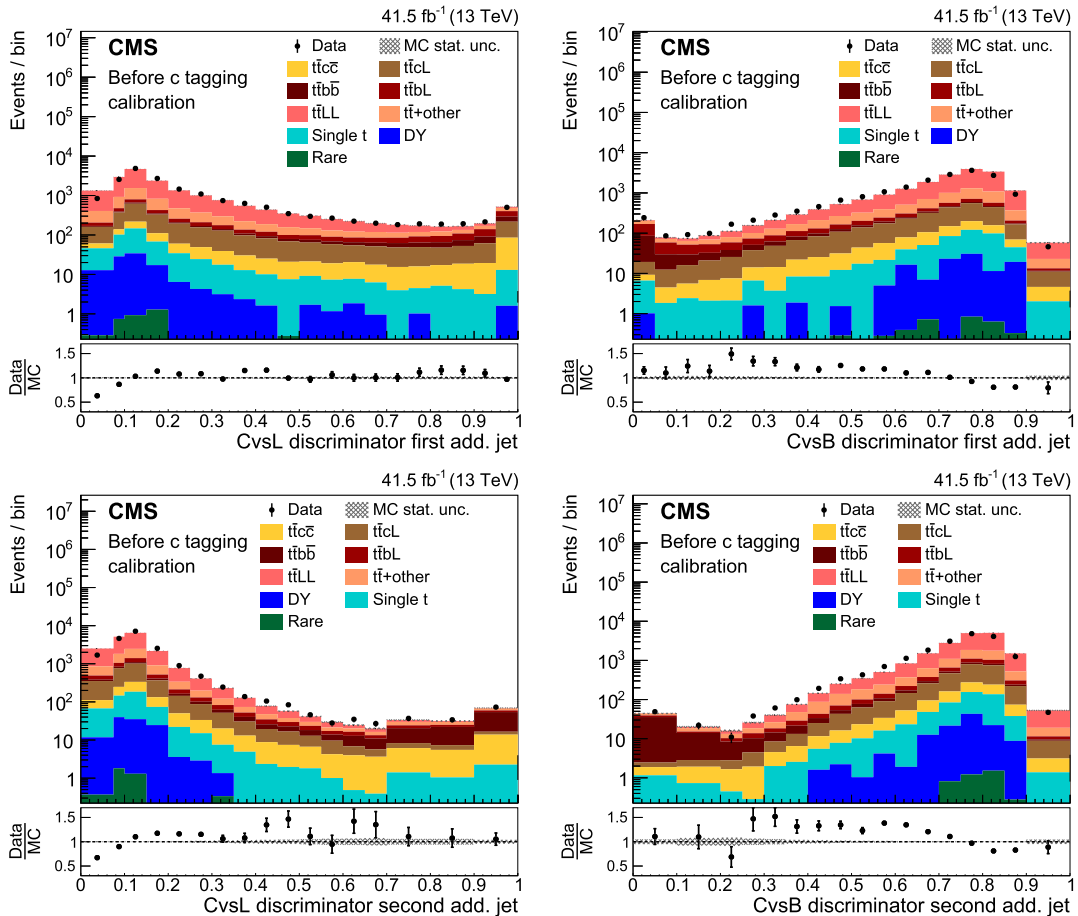


Fig. 7. Comparison between data (points) and simulated predictions (histograms) for the CvsL (left column) and CvsB (right column) c tagging discriminator distributions of the first (upper row) and second (lower row) additional jet before applying the c tagging calibration. The lower panels show the ratio of the yields in data to those predicted in simulations. The vertical bars represent the statistical uncertainties in data, while the hatched bands show the statistical uncertainty in the simulated predictions.

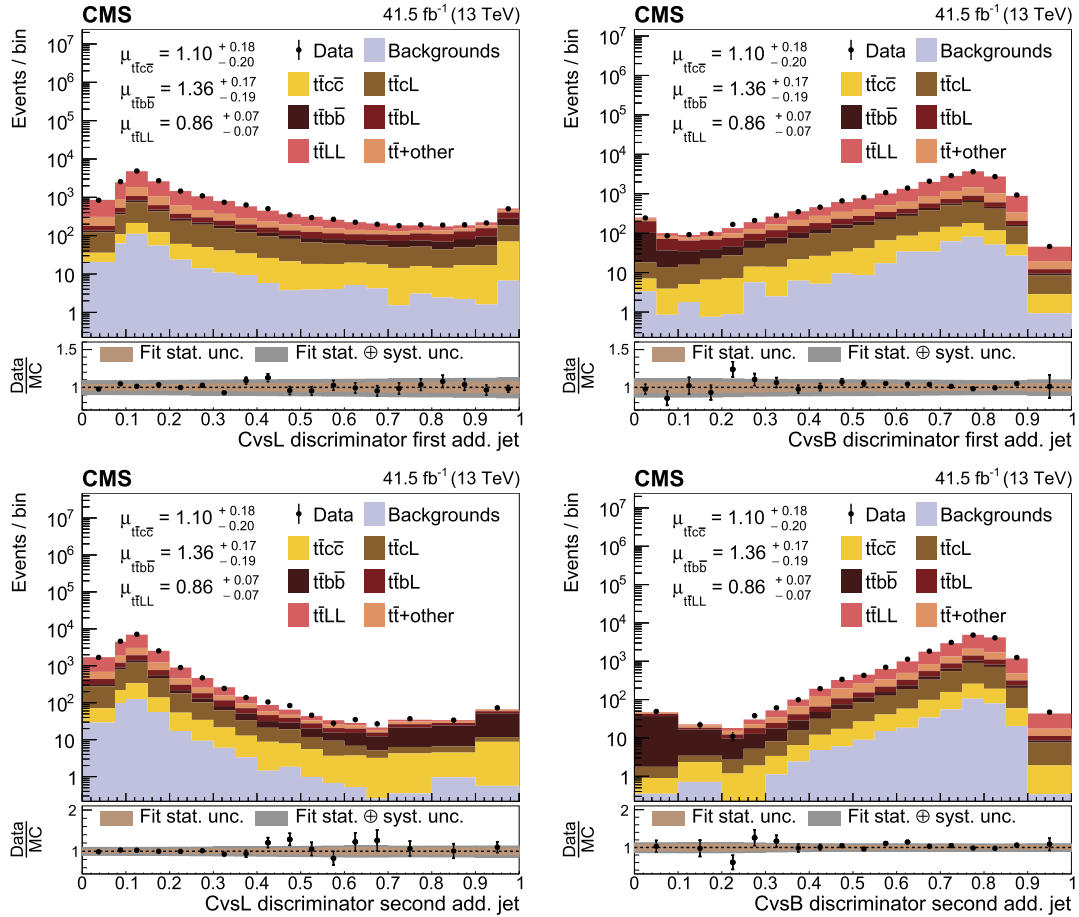


Fig. 8. Comparison between data (points) and simulated predictions (histograms) for the CvsL (left column) and CvsB (right column) c tagging discriminator distributions of the first (upper row) and second (lower row) additional jet, after normalizing the simulated templates according to the fitted cross sections. The lower panels show the ratio of the yields in data to those predicted in the simulations. The brown and grey uncertainty bands denote, respectively, the statistical and total uncertainties from the fit. The factors (μ) by which the templates of the different processes (using the POWHEG ME generator) are scaled, are also displayed, together with their combined statistical and systematic uncertainties.

ME level, is interfaced with a parton shower simulation to generate the additional radiation. Agreement is observed at the level of one to two standard deviations between the measured values and simulated predictions for the $t\bar{t}c\bar{c}$, $t\bar{t}b\bar{b}$, and $t\bar{t}LL$ processes. The observed ratio of the $t\bar{t}b\bar{b}$ to the inclusive $t\bar{t}$ + two jets cross sections exceeds the predictions by about 2.5 standard deviations, consistent with the tendency seen in previous measurements.

Declaration of competing interest

The authors declare that they have no known competing financial interests or personal relationships that could have appeared to influence the work reported in this paper.

Acknowledgements

We congratulate our colleagues in the CERN accelerator departments for the excellent performance of the LHC and thank the technical and administrative staffs at CERN and at other CMS institutes for their contributions to the success of the CMS effort. In addition, we gratefully acknowledge the computing centres and personnel of the Worldwide LHC Computing Grid for delivering so effectively the computing infrastructure essential to our analyses. Finally, we acknowledge the enduring support for the construction and operation of the LHC and the CMS detector provided by the following funding agencies: BMBWF and FWF (Austria); FNRS and FWO (Belgium); CNPq, CAPES, FAPERJ, FAPERGS, and FAPESP

(Brazil); MES (Bulgaria); CERN; CAS, MOST, and NSFC (China); COLCIENCIAS (Colombia); MSES and CSF (Croatia); RIF (Cyprus); SENESCYT (Ecuador); MoER, ERC PUT and ERDF (Estonia); Academy of Finland, MEC, and HIP (Finland); CEA and CNRS/IN2P3 (France); BMBF, DFG, and HGF (Germany); GSRT (Greece); NKfIA (Hungary); DAE and DST (India); IPM (Iran); SFI (Ireland); INFN (Italy); MSIP and NRF (Republic of Korea); MES (Latvia); LAS (Lithuania); MOE and UM (Malaysia); BUAP, CINVESTAV, CONACYT, LNS, SEP, and UASLP-FAI (Mexico); MOS (Montenegro); MBIE (New Zealand); PAEC (Pakistan); MSHE and NSC (Poland); FCT (Portugal); JINR (Dubna); MON, ROSATOM, RAS, RFBR, and NRC KI (Russia); MESTD (Serbia); SEIDI, CPAN, PCTI, and FEDER (Spain); MoSTR (Sri Lanka); Swiss Funding Agencies (Switzerland); MST (Taipei); ThEPCenter, IPST, STAR, and NSTDA (Thailand); TUBITAK and TAEK (Turkey); NASU (Ukraine); STFC (United Kingdom); DOE and NSF (USA).

Individuals have received support from the Marie-Curie programme and the European Research Council and Horizon 2020 Grant, contract Nos. 675440, 724704, 752730, and 765710 (European Union); the Leventis Foundation; the A.P. Sloan Foundation; the Alexander von Humboldt Foundation; the Belgian Federal Science Policy Office; the Fonds pour la Formation à la Recherche dans l'Industrie et dans l'Agriculture (FRIA-Belgium); the Agentschap voor Innovatie door Wetenschap en Technologie (IWT-Belgium); the F.R.S.-FNRS and FWO (Belgium) under the "Excellence of Science – EOS" – be.h project n. 30820817; the Beijing Municipal Science & Technology Commission, No. Z191100007219010; the Ministry of Education, Youth and Sports

(MEYS) of the Czech Republic; the Deutsche Forschungsgemeinschaft (DFG) under Germany's Excellence Strategy – EXC 2121 “Quantum Universe” – 390833306; the Lendület (“Momentum”) Programme and the János Bolyai Research Scholarship of the Hungarian Academy of Sciences, the New National Excellence Program ÚNKP, the NKFI research grants 123842, 123959, 124845, 124850, 125105, 128713, 128786, and 129058 (Hungary); the Council of Science and Industrial Research, India; the HOMING PLUS programme of the Foundation for Polish Science, cofinanced from European Union, Regional Development Fund, the Mobility Plus programme of the Ministry of Science and Higher Education, the National Science Center (Poland), contracts Harmonia 2014/14/M/ST2/00428, Opus 2014/13/B/ST2/02543, 2014/15/B/ST2/03998, and 2015/19/B/ST2/02861, Sonata-bis 2012/07/E/ST2/01406; the National Priorities Research Program by Qatar National Research Fund; the Ministry of Science and Higher Education, project no. 0723-2020-0041 (Russia); the Tomsk Polytechnic University Competitiveness Enhancement Program; the Programa Estatal de Fomento de la Investigación Científica y Técnica de Excelencia María de Maeztu, grant MDM-2015-0509 and the Programa Severo Ochoa del Principado de Asturias; the Thalís and Aristeia programmes cofinanced by EU-ESF and the Greek NSRF; the Rachadapisek Sompot Fund for Postdoctoral Fellowship, Chulalongkorn University and the Chulalongkorn Academic into Its 2nd Century Project Advancement Project (Thailand); the Kavli Foundation; the Nvidia Corporation; the SuperMicro Corporation; the Welch Foundation, contract C-1845; and the Weston Havens Foundation (USA).

Appendix A. Charm tagging discriminators before calibration

The c tagging algorithms are trained on simulated events and are therefore prone to mismodelling effects in the input variables. The initial C_{vsL} and C_{vsB} c tagging discriminator distributions of the first and second additional jet are shown in Fig. 7. Discrepancies between the data and the simulated predictions of up to 50% are observed, demonstrating the need for the c tagging calibration described in Section 8.

Appendix B. Charm tagging discriminators after scaling to the fitted cross sections

After scaling the simulated templates of the c tagging discriminators to their fitted yields, the agreement between data and simulations is shown in Fig. 8. This can be compared to the agreement before the fit was performed in Fig. 3, and indeed shows an improved agreement especially in those bins which have a relatively large contribution from $t\bar{t}b\bar{b}$ and $t\bar{t}c\bar{c}$ events.

References

- [1] A. Bredenstein, A. Denner, S. Dittmaier, S. Pozzorini, NLO QCD corrections to $t\bar{t}b\bar{b}$ production at the LHC: 1. Quark-antiquark annihilation, *J. High Energy Phys.* 08 (2008) 108, <https://doi.org/10.1088/1126-6708/2008/08/108>, arXiv:0807.1248.
- [2] A. Bredenstein, A. Denner, S. Dittmaier, S. Pozzorini, NLO QCD corrections to $pp \rightarrow t\bar{t}b\bar{b} + X$ at the LHC, *Phys. Rev. Lett.* 103 (2009) 012002, <https://doi.org/10.1103/PhysRevLett.103.012002>, arXiv:0905.0110.
- [3] F. Cascioli, P. Maierhöfer, N. Moretti, S. Pozzorini, F. Siegert, NLO matching for $t\bar{t}b\bar{b}$ production with massive b quarks, *Phys. Lett. B* 734 (2014) 210, <https://doi.org/10.1016/j.physletb.2014.05.040>, arXiv:1309.5912.
- [4] T. Ježo, J.M. Lindert, N. Moretti, S. Pozzorini, New NLOPS predictions for $t\bar{t} + b$ jet production at the LHC, *Eur. Phys. J. C* 78 (2018) 502, <https://doi.org/10.1140/epjc/s10052-018-5956-0>, arXiv:1802.00426.
- [5] F. Buccioni, S. Kallweit, S. Pozzorini, M.F. Zoller, NLO QCD predictions for $t\bar{t}b\bar{b}$ production in association with a light jet at the LHC, *J. High Energy Phys.* 12 (2019) 015, [https://doi.org/10.1007/JHEP12\(2019\)015](https://doi.org/10.1007/JHEP12(2019)015), arXiv:1907.13624.
- [6] ATLAS Collaboration, Study of heavy-flavour quarks produced in association with top quark pairs at $\sqrt{s} = 7$ TeV using the ATLAS detector, *Phys. Rev. D* 89 (2014) 072012, <https://doi.org/10.1103/PhysRevD.89.072012>, arXiv:1304.6386.
- [7] CMS Collaboration, Measurement of the cross section ratio $\sigma_{t\bar{t}b\bar{b}}/\sigma_{t\bar{t}ij}$ in pp collisions at $\sqrt{s} = 8$ TeV, *Phys. Lett. B* 746 (2015) 132, <https://doi.org/10.1016/j.physletb.2015.04.060>, arXiv:1411.5621.
- [8] ATLAS Collaboration, Measurements of fiducial cross sections for $t\bar{t}$ production with one or two additional b jets in pp collisions at $\sqrt{s} = 8$ TeV using the ATLAS detector, *Eur. Phys. J. C* 76 (2016) 11, <https://doi.org/10.1140/epjc/s10052-015-3852-4>, arXiv:1508.06868.
- [9] CMS Collaboration, Measurement of $t\bar{t}$ production with additional jet activity, including b quark jets, in the dilepton decay channel using pp collisions at $\sqrt{s} = 8$ TeV, *Eur. Phys. J. C* 76 (2016) 379, <https://doi.org/10.1140/epjc/s10052-016-4105-x>, arXiv:1510.03072.
- [10] CMS Collaboration, Measurements of $t\bar{t}$ cross sections in association with b jets and inclusive jets and their ratio using dilepton final states in pp collisions at $\sqrt{s} = 13$ TeV, *Phys. Lett. B* 776 (2018) 355, <https://doi.org/10.1016/j.physletb.2017.11.043>, arXiv:1705.10141.
- [11] ATLAS Collaboration, Measurements of inclusive and differential fiducial cross sections of $t\bar{t}$ production with additional heavy-flavour jets in proton-proton collisions at $\sqrt{s} = 13$ TeV with the ATLAS detector, *J. High Energy Phys.* 04 (2019) 046, [https://doi.org/10.1007/JHEP04\(2019\)046](https://doi.org/10.1007/JHEP04(2019)046), arXiv:1811.12113.
- [12] CMS Collaboration, Measurement of the $t\bar{t}b\bar{b}$ production cross section in the all-jet final state in pp collisions at $\sqrt{s} = 13$ TeV, *Phys. Lett. B* 803 (2020) 135285, <https://doi.org/10.1016/j.physletb.2020.135285>, arXiv:1909.05306.
- [13] CMS Collaboration, Measurement of the cross section for $t\bar{t}$ production with additional jets and b jets in pp collisions at $\sqrt{s} = 13$ TeV, *J. High Energy Phys.* 07 (2020) 125, [https://doi.org/10.1007/JHEP07\(2020\)125](https://doi.org/10.1007/JHEP07(2020)125), arXiv:2003.06467.
- [14] CMS Collaboration, Identification of heavy-flavour jets with the CMS detector in pp collisions at 13 TeV, *J. Instrum.* 13 (2018) P05011, <https://doi.org/10.1088/1748-0221/13/05/P05011>, arXiv:1712.07158.
- [15] CMS Collaboration, CMS luminosity measurement for the 2017 data-taking period at $\sqrt{s} = 13$ TeV, CMS Physics Analysis Summary CMS-PAS-LUM-17-004, CERN, <https://cds.cern.ch/record/2621960>, 2018.
- [16] CMS Collaboration, CMS technical design report for the pixel detector upgrade, CMS Technical Design Report CERN-LHCC-2012-016, CMS-TDR-011, CERN, 2012, <https://cds.cern.ch/record/1481838>.
- [17] CMS Collaboration, Performance of b tagging algorithms in proton-proton collisions at 13 TeV with Phase 1 CMS detector, CMS Detector Performance Note CMS-DP-2018-033, CERN, <https://cds.cern.ch/record/2627468>, 2018.
- [18] CMS Collaboration, Observation of $t\bar{t}H$ production, *Phys. Rev. Lett.* 120 (2018) 231801, <https://doi.org/10.1103/PhysRevLett.120.231801>, arXiv:1804.02610.
- [19] CMS Collaboration, Search for $t\bar{t}H$ production in the $H \rightarrow b\bar{b}$ decay channel with leptonic $t\bar{t}$ decays in proton-proton collisions at $\sqrt{s} = 13$ TeV, *J. High Energy Phys.* 03 (2019) 026, [https://doi.org/10.1007/JHEP03\(2019\)026](https://doi.org/10.1007/JHEP03(2019)026), arXiv:1804.03682.
- [20] ATLAS Collaboration, Observation of Higgs boson production in association with a top quark pair at the LHC with the ATLAS detector, *Phys. Lett. B* 784 (2018) 173, <https://doi.org/10.1016/j.physletb.2018.07.035>, arXiv:1806.00425.
- [21] ATLAS Collaboration, Search for the standard model Higgs boson produced in association with top quarks and decaying into a $b\bar{b}$ pair in pp collisions at $\sqrt{s} = 13$ TeV with the ATLAS detector, *Phys. Rev. D* 97 (2018) 072016, <https://doi.org/10.1103/PhysRevD.97.072016>, arXiv:1712.08895.
- [22] CMS Collaboration, Track impact parameter resolution in the 2017 dataset with the CMS phase-1 pixel detector, CMS Detector Performance Note CMS-DP-2020-032, CERN, <https://cds.cern.ch/record/2723305>, 2020.
- [23] CMS Collaboration, The CMS experiment at the CERN LHC, *J. Instrum.* 3 (2008) S08004, <https://doi.org/10.1088/1748-0221/3/08/S08004>.
- [24] CMS Collaboration, The CMS trigger system, *J. Instrum.* 12 (2017) P01020, <https://doi.org/10.1088/1748-0221/12/01/P01020>, arXiv:1609.02366.
- [25] P. Nason, A new method for combining NLO QCD with shower Monte Carlo algorithms, *J. High Energy Phys.* 11 (2004) 040, <https://doi.org/10.1088/1126-6708/2004/11/040>, arXiv:hep-ph/0409146.
- [26] S. Frixione, P. Nason, C. Oleari, Matching NLO QCD computations with parton shower simulations: the powheg method, *J. High Energy Phys.* 11 (2007) 070, <https://doi.org/10.1088/1126-6708/2007/11/070>, arXiv:0709.2092.
- [27] S. Alioli, P. Nason, C. Oleari, E. Re, A general framework for implementing NLO calculations in shower Monte Carlo programs: the powheg BOX, *J. High Energy Phys.* 06 (2010) 043, [https://doi.org/10.1007/JHEP06\(2010\)043](https://doi.org/10.1007/JHEP06(2010)043), arXiv:1002.2581.
- [28] J.M. Campbell, R.K. Ellis, P. Nason, E. Re, Top-pair production and decay at NLO matched with parton showers, *J. High Energy Phys.* 04 (2015) 114, [https://doi.org/10.1007/JHEP04\(2015\)114](https://doi.org/10.1007/JHEP04(2015)114), arXiv:1412.1828.
- [29] S. Frixione, P. Nason, G. Ridolfi, A positive-weight next-to-leading-order Monte Carlo for heavy-flavour hadroproduction, *J. High Energy Phys.* 09 (2007) 126, <https://doi.org/10.1088/1126-6708/2007/09/126>, arXiv:0707.3088.
- [30] T. Sjöstrand, S. Ask, J.R. Christiansen, R. Corke, N. Desai, P. Ilten, S. Mrenna, S. Prestel, C.O. Rasmussen, P.Z. Skands, An introduction to PYTHIA8.2, *Comput. Phys. Commun.* 191 (2015) 159, <https://doi.org/10.1016/j.cpc.2015.01.024>, arXiv:1410.3012.
- [31] CMS Collaboration, Extraction and validation of a new set of CMS PYTHIA8 tunes from underlying-event measurements, *Eur. Phys. J. C* 80 (2020) 4, <https://doi.org/10.1140/epjc/s10052-019-7499-4>, arXiv:1903.12179.

- [32] R.D. Ball, et al., NNPDF, Parton distributions from high-precision collider data, *Eur. Phys. J. C* 77 (2017) 663, <https://doi.org/10.1140/epjc/s10052-017-5199-5>, arXiv:1706.00428.
- [33] M. Cacciari, M. Czakon, M. Mangano, A. Mitov, P. Nason, Top-pair production at hadron colliders with next-to-next-to-leading logarithmic soft-gluon resummation, *Phys. Lett. B* 710 (2012) 612, <https://doi.org/10.1016/j.physletb.2012.03.013>, arXiv:1111.5869.
- [34] J. Alwall, R. Frederix, S. Frixione, V. Hirschi, F. Maltoni, O. Mattelaer, H.S. Shao, T. Stelzer, P. Torrielli, M. Zaro, The automated computation of tree-level and next-to-leading order differential cross sections, and their matching to parton shower simulations, *J. High Energy Phys.* 07 (2014) 079, [https://doi.org/10.1007/JHEP07\(2014\)079](https://doi.org/10.1007/JHEP07(2014)079), arXiv:1405.0301.
- [35] R. Frederix, S. Frixione, Merging meets matching in MC@NLO, *J. High Energy Phys.* 12 (2012) 061, [https://doi.org/10.1007/JHEP12\(2012\)061](https://doi.org/10.1007/JHEP12(2012)061), arXiv:1209.6215.
- [36] J. Alwall, S. Höche, F. Krauss, N. Lavesson, L. Lonnblad, F. Maltoni, M.L. Mangano, M. Moretti, C.G. Papadopoulos, F. Piccinini, S. Schumann, M. Treccani, J. Winter, M. Worek, Comparative study of various algorithms for the merging of parton showers and matrix elements in hadronic collisions, *Eur. Phys. J. C* 53 (2008) 473, <https://doi.org/10.1140/epjc/s10052-007-0490-5>, arXiv:0706.2569.
- [37] S. Agostinelli, et al., GEANT4, Geant4 – a simulation toolkit, *Nucl. Instrum. Methods A* 506 (2003) 250, [https://doi.org/10.1016/S0168-9002\(03\)01368-8](https://doi.org/10.1016/S0168-9002(03)01368-8).
- [38] M. Cacciari, G.P. Salam, Pileup subtraction using jet areas, *Phys. Lett. B* 659 (2008) 119, <https://doi.org/10.1016/j.physletb.2007.09.077>, arXiv:0707.1378.
- [39] M. Cacciari, G.P. Salam, G. Soyez, The anti- k_T jet clustering algorithm, *J. High Energy Phys.* 04 (2008) 063, <https://doi.org/10.1088/1126-6708/2008/04/063>, arXiv:0802.1189.
- [40] M. Cacciari, G.P. Salam, G. Soyez, FastJet user manual, *Eur. Phys. J. C* 72 (2012) 1896, <https://doi.org/10.1140/epjc/s10052-012-1896-2>, arXiv:1111.6097.
- [41] CMS Collaboration, Particle-flow reconstruction and global event description with the CMS detector, *J. Instrum.* 12 (2017) P10003, <https://doi.org/10.1088/1748-0221/12/10/P10003>, arXiv:1706.04965.
- [42] CMS Collaboration, Jet energy scale and resolution in the CMS experiment in pp collisions at 8 TeV, *J. Instrum.* 12 (2017) P02014, <https://doi.org/10.1088/1748-0221/12/02/P02014>, arXiv:1607.03663.
- [43] CMS Collaboration, Performance of missing transverse momentum reconstruction in proton-proton collisions at $\sqrt{s} = 13$ TeV using the CMS detector, *J. Instrum.* 14 (2019) P07004, <https://doi.org/10.1088/1748-0221/14/07/P07004>, arXiv:1903.06078.
- [44] Particle Data Group, P.A. Zyla, et al., Review of particle physics, *Prog. Theor. Exp. Phys.* 2020 (2020) 083C01, <https://doi.org/10.1093/ptep/ptaa104>.
- [45] F. Chollet, et al., <https://github.com/keras-team/keras>, 2015, software available from GitHub.
- [46] A. Martín, et al., TensorFlow: large-scale machine learning on heterogeneous systems, software available from <https://www.tensorflow.org/>, 2015.
- [47] CMS Collaboration, Calibration of charm jet identification algorithms using proton-proton collision events at $\sqrt{s} = 13$ TeV, CMS Physics Analysis Summary CMS-PAS-BTV-20-001, CERN, <https://cds.cern.ch/record/2758866>, 2021.
- [48] G. Aad, et al., ATLAS, CMS, Measurements of the Higgs boson production and decay rates and constraints on its couplings from a combined ATLAS and CMS analysis of the LHC pp collision data at $\sqrt{s} = 7$ and 8 TeV, *J. High Energy Phys.* 08 (2016) 045, [https://doi.org/10.1007/JHEP08\(2016\)045](https://doi.org/10.1007/JHEP08(2016)045), arXiv:1606.02266.
- [49] CMS Collaboration, Precise determination of the mass of the Higgs boson and tests of compatibility of its couplings with the standard model predictions using proton collisions at 7 and 8 TeV, *Eur. Phys. J. C* 75 (2015) 212, <https://doi.org/10.1140/epjc/s10052-015-3351-7>, arXiv:1412.8662.
- [50] A. Savitzky, M. Golay, Smoothing and differentiation of data by simplified least squares procedures, *Anal. Chem.* 36 (1964) 1627, <https://doi.org/10.1021/ac60214a047>.
- [51] CMS Collaboration, Measurement of the inelastic proton-proton cross section at $\sqrt{s} = 13$ TeV, *J. High Energy Phys.* 07 (2018) 161, [https://doi.org/10.1007/JHEP07\(2018\)161](https://doi.org/10.1007/JHEP07(2018)161), arXiv:1802.02613.
- [52] M. Cacciari, S. Frixione, M.L. Mangano, P. Nason, G. Ridolfi, The $t\bar{t}$ cross section at 1.8 and 1.96 TeV: a study of the systematics due to parton densities and scale dependence, *J. High Energy Phys.* 04 (2004) 068, <https://doi.org/10.1088/1126-6708/2004/04/068>, arXiv:hep-ph/0303085.
- [53] S. Catani, D. de Florian, M. Grazzini, P. Nason, Soft gluon resummation for Higgs boson production at hadron colliders, *J. High Energy Phys.* 07 (2003) 028, <https://doi.org/10.1088/1126-6708/2003/07/028>, arXiv:hep-ph/0306211.
- [54] M.G. Bowler, e^+e^- production of heavy quarks in the string model, *Z. Phys. C* 11 (1981) 169, <https://doi.org/10.1007/BF01574001>.
- [55] B. Andersson, G. Gustafson, G. Ingelman, T. Sjöstrand, Parton fragmentation and string dynamics, *Phys. Rep.* 97 (1983) 31, [https://doi.org/10.1016/0370-1573\(83\)90080-7](https://doi.org/10.1016/0370-1573(83)90080-7).
- [56] T. Sjöstrand, Jet fragmentation of nearby partons, *Nucl. Phys. B* 248 (1984) 469, [https://doi.org/10.1016/0550-3213\(84\)90607-2](https://doi.org/10.1016/0550-3213(84)90607-2).
- [57] A. Heister, et al., ALEPH, Study of the fragmentation of b quarks into B mesons at the Z peak, *Phys. Lett. B* 512 (2001) 30, [https://doi.org/10.1016/S0370-2693\(01\)00690-6](https://doi.org/10.1016/S0370-2693(01)00690-6), arXiv:hep-ex/0106051.
- [58] J. Abdallah, et al., DELPHI, A study of the b quark fragmentation function with the DELPHI detector at LEP I and an averaged distribution obtained at the Z pole, *Eur. Phys. J. C* 71 (2011) 1557, <https://doi.org/10.1140/epjc/s10052-011-1557-x>, arXiv:1102.4748.
- [59] G. Abbiendi, et al., OPAL, Inclusive analysis of the b quark fragmentation function in Z decays at LEP, *Eur. Phys. J. C* 29 (2003) 463, <https://doi.org/10.1140/epjc/s2003-01229-x>, arXiv:hep-ex/0210031.
- [60] K. Abe, et al., SLD, Measurement of the b quark fragmentation function in Z^0 decays, *Phys. Rev. D* 65 (2002) 092006, <https://doi.org/10.1103/PhysRevD.66.079905>, arXiv:hep-ex/0202031.
- [61] R. Barate, et al., ALEPH, Study of charm production in Z decays, *Eur. Phys. J. C* 16 (2000) 597, <https://doi.org/10.1007/s100520000421>, arXiv:hep-ex/9909032.
- [62] P. Skands, S. Carrazza, J. Rojo, Tuning pythia 8.1: the Monash 2013 tune, *Eur. Phys. J. C* 74 (2014) 3024, <https://doi.org/10.1140/epjc/s10052-014-3024-y>, arXiv:1404.5630.
- [63] J. Butterworth, et al., PDF4LHC recommendations for LHC run II, *J. Phys. G* 43 (2016) 023001, <https://doi.org/10.1088/0954-3889/43/2/023001>, arXiv:1510.03865.
- [64] CMS Collaboration, Electroweak production of two jets in association with a Z boson in proton-proton collisions at $\sqrt{s} = 13$ TeV, *Eur. Phys. J. C* 78 (2018) 589, <https://doi.org/10.1140/epjc/s10052-018-6049-9>, arXiv:1712.09814.
- [65] CMS Collaboration, Measurement of the single top quark and antiquark production cross sections in the t channel and their ratio in proton-proton collisions at $\sqrt{s} = 13$ TeV, *Phys. Lett. B* 800 (2020) 135042, <https://doi.org/10.1016/j.physletb.2019.135042>, arXiv:1812.10514.

The CMS Collaboration

A.M. Sirunyan[†], A. Tumasyan

Yerevan Physics Institute, Yerevan, Armenia

W. Adam, T. Bergauer, M. Dragicevic, A. Escalante Del Valle, R. Frühwirth¹, M. Jeitler¹, N. Krammer, L. Lechner, D. Liko, I. Mikulec, F.M. Pitters, J. Schieck¹, R. Schöfbeck, M. Spanring, S. Templ, W. Waltenberger, C.-E. Wulz¹, M. Zarucki

Institut für Hochenergiephysik, Wien, Austria

V. Chekhovsky, A. Litomin, V. Makarenko

Institute for Nuclear Problems, Minsk, Belarus

M.R. Darwish², E.A. De Wolf, X. Janssen, T. Kello³, A. Lelek, M. Pieters, H. Rejeb Sfar, P. Van Mechelen, S. Van Putte, N. Van Remortel

Universiteit Antwerpen, Antwerpen, Belgium

F. Blekman, E.S. Bols, J. D'Hondt, J. De Clercq, D. Lontkovskyi, S. Lowette, I. Marchesini, S. Moortgat, A. Morton, D. Müller, A.R. Sahasransu, S. Tavernier, W. Van Doninck, P. Van Mulders

Vrije Universiteit Brussel, Brussel, Belgium

D. Beghin, B. Bilin, B. Clerbaux, G. De Lentdecker, B. Dorney, L. Favart, A. Grebenyuk, A.K. Kalsi, K. Lee, I. Makarenko, L. Moureaux, L. Pétré, A. Popov, N. Postiau, E. Starling, L. Thomas, C. Vander Velde, P. Vanlaer, D. Vannerom, L. Wezenbeek

Université Libre de Bruxelles, Bruxelles, Belgium

T. Cornelis, D. Dobur, M. Gruchala, I. Khvastunov⁴, G. Mestdach, M. Niedziela, C. Roskas, K. Skovpen, M. Tytgat, W. Verbeke, B. Vermassen, M. Vit

Ghent University, Ghent, Belgium

A. Bethani, G. Bruno, F. Bury, C. Caputo, P. David, C. Delaere, M. Delcourt, I.S. Donertas, A. Giammanco, V. Lemaître, K. Mondal, J. Prisciandaro, A. Taliercio, M. Teklishyn, P. Vischia, S. Wertz, S. Wuyckens

Université Catholique de Louvain, Louvain-la-Neuve, Belgium

G.A. Alves, C. Hensel, A. Moraes

Centro Brasileiro de Pesquisas Físicas, Rio de Janeiro, Brazil

W.L. Aldá Júnior, E. Belchior Batista Das Chagas, H. Brandao Malbouisson, W. Carvalho, J. Chinellato⁵, E. Coelho, E.M. Da Costa, G.G. Da Silveira⁶, D. De Jesus Damiao, S. Fonseca De Souza, J. Martins⁷, D. Matos Figueiredo, C. Mora Herrera, L. Mundim, H. Nogima, P. Rebello Teles, L.J. Sanchez Rosas, A. Santoro, S.M. Silva Do Amaral, A. Sznajder, M. Thiel, F. Torres Da Silva De Araujo, A. Vilela Pereira

Universidade do Estado do Rio de Janeiro, Rio de Janeiro, Brazil

C.A. Bernardes^a, L. Calligaris^a, T.R. Fernandez Perez Tomei^a, E.M. Gregores^{a,b}, D.S. Lemos^a, P.G. Mercadante^{a,b}, S.F. Novaes^a, Sandra S. Padula^a

^a *Universidade Estadual Paulista, São Paulo, Brazil*

^b *Universidade Federal do ABC, São Paulo, Brazil*

A. Aleksandrov, G. Antchev, I. Atanasov, R. Hadjiiska, P. Iaydjiev, M. Misheva, M. Rodozov, M. Shopova, G. Sultanov

Institute for Nuclear Research and Nuclear Energy, Bulgarian Academy of Sciences, Sofia, Bulgaria

A. Dimitrov, T. Ivanov, L. Litov, B. Pavlov, P. Petkov, A. Petrov

University of Sofia, Sofia, Bulgaria

T. Cheng, W. Fang³, Q. Guo, M. Mittal, H. Wang, L. Yuan

Beihang University, Beijing, China

M. Ahmad, G. Bauer, Z. Hu, Y. Wang, K. Yi^{8,9}

Department of Physics, Tsinghua University, Beijing, China

E. Chapon, G.M. Chen¹⁰, H.S. Chen¹⁰, M. Chen, T. Javaid¹⁰, A. Kapoor, D. Leggat, H. Liao, Z.-A. Liu¹⁰, R. Sharma, A. Spiezia, J. Tao, J. Thomas-Wilsker, J. Wang, H. Zhang, S. Zhang¹⁰, J. Zhao

Institute of High Energy Physics, Beijing, China

A. Agapitos, Y. Ban, C. Chen, Q. Huang, A. Levin, Q. Li, M. Lu, X. Lyu, Y. Mao, S.J. Qian, D. Wang, Q. Wang, J. Xiao

State Key Laboratory of Nuclear Physics and Technology, Peking University, Beijing, China

Z. You

Sun Yat-Sen University, Guangzhou, China

X. Gao³, H. Okawa

Institute of Modern Physics and Key Laboratory of Nuclear Physics and Ion-beam Application (MOE) – Fudan University, Shanghai, China

M. Xiao

Zhejiang University, Hangzhou, China

C. Avila, A. Cabrera, C. Florez, J. Fraga, A. Sarkar, M.A. Segura Delgado

Universidad de Los Andes, Bogota, Colombia

J. Jaramillo, J. Mejia Guisao, F. Ramirez, J.D. Ruiz Alvarez, C.A. Salazar González, N. Vanegas Arbelaez

Universidad de Antioquia, Medellin, Colombia

D. Giljanovic, N. Godinovic, D. Lelas, I. Puljak

University of Split, Faculty of Electrical Engineering, Mechanical Engineering and Naval Architecture, Split, Croatia

Z. Antunovic, M. Kovac, T. Sculac

University of Split, Faculty of Science, Split, Croatia

V. Brigljevic, D. Ferencek, D. Majumder, M. Roguljic, A. Starodumov¹¹, T. Susa

Institute Rudjer Boskovic, Zagreb, Croatia

M.W. Ather, A. Attikis, E. Erodotou, A. Ioannou, G. Kole, M. Kolosova, S. Konstantinou, J. Mousa, C. Nicolaou, F. Ptochos, P.A. Razis, H. Rykaczewski, H. Saka, D. Tsiakkouri

University of Cyprus, Nicosia, Cyprus

M. Finger¹², M. Finger Jr.¹², A. Kveton, J. Tomsa

Charles University, Prague, Czech Republic

E. Ayala

Escuela Politecnica Nacional, Quito, Ecuador

E. Carrera Jarrin

Universidad San Francisco de Quito, Quito, Ecuador

A.A. Abdelalim^{13,14}, S. Abu Zeid¹⁵, S. Elgammal¹⁶

Academy of Scientific Research and Technology of the Arab Republic of Egypt, Egyptian Network of High Energy Physics, Cairo, Egypt

M.A. Mahmoud, Y. Mohammed

Center for High Energy Physics (CHEP-FU), Fayoum University, El-Fayoum, Egypt

S. Bhowmik, A. Carvalho Antunes De Oliveira, R.K. Dewanjee, K. Ehataht, M. Kadastik, J. Pata, M. Raidal, C. Veelken

National Institute of Chemical Physics and Biophysics, Tallinn, Estonia

P. Eerola, L. Forthomme, H. Kirschenmann, K. Osterberg, M. Voutilainen

Department of Physics, University of Helsinki, Helsinki, Finland

E. Brücken, F. Garcia, J. Havukainen, V. Karimäki, M.S. Kim, R. Kinnunen, T. Lampén, K. Lassila-Perini, S. Lehti, T. Lindén, H. Siikonen, E. Tuominen, J. Tuominiemi

Helsinki Institute of Physics, Helsinki, Finland

P. Luukka, T. Tuuva

Lappeenranta University of Technology, Lappeenranta, Finland

C. Amendola, M. Besancon, F. Couderc, M. Dejardin, D. Denegri, J.L. Faure, F. Ferri, S. Ganjour, A. Givernaud, P. Gras, G. Hamel de Monchenault, P. Jarry, B. Lenzi, E. Locci, J. Malcles, J. Rander, A. Rosowsky, M.Ö. Sahin, A. Savoy-Navarro¹⁷, M. Titov, G.B. Yu

IRFU, CEA, Université Paris-Saclay, Gif-sur-Yvette, France

S. Ahuja, F. Beaudette, M. Bonanomi, A. Buchot Perraguin, P. Busson, C. Charlot, O. Davignon, B. Diab, G. Falmagne, R. Granier de Cassagnac, A. Hakimi, I. Kucher, A. Lobanov, C. Martin Perez, M. Nguyen, C. Ochando, P. Paganini, J. Rembser, R. Salerno, J.B. Sauvan, Y. Sirois, A. Zabi, A. Zghiche

Laboratoire Leprince-Ringuet, CNRS/IN2P3, Ecole Polytechnique, Institut Polytechnique de Paris, Palaiseau, France

J.-L. Agram¹⁸, J. Andrea, D. Bloch, G. Bourgatte, J.-M. Brom, E.C. Chabert, C. Collard, J.-C. Fontaine¹⁸, U. Goerlach, C. Grimault, A.-C. Le Bihan, P. Van Hove

Université de Strasbourg, CNRS, IPHC UMR 7178, Strasbourg, France

E. Asilar, S. Beauceron, C. Bernet, G. Boudoul, C. Camen, A. Carle, N. Chanon, D. Contardo, P. Depasse, H. El Mamouni, J. Fay, S. Gascon, M. Gouzevitch, B. Ille, Sa. Jain, I.B. Laktineh, H. Lattaud, A. Lesauvage, M. Lethuillier, L. Mirabito, K. Shchablo, L. Torterotot, G. Touquet, M. Vander Donckt, S. Viret

Université de Lyon, Université Claude Bernard Lyon 1, CNRS-IN2P3, Institut de Physique Nucléaire de Lyon, Villeurbanne, France

A. Khvedelidze¹², Z. Tsamalaidze¹²

Georgian Technical University, Tbilisi, Georgia

L. Feld, K. Klein, M. Lipinski, D. Meuser, A. Pauls, M.P. Rauch, J. Schulz, M. Teroerde

RWTH Aachen University, I. Physikalisches Institut, Aachen, Germany

D. Eliseev, M. Erdmann, P. Fackeldey, B. Fischer, S. Ghosh, T. Hebbeker, K. Hoepfner, H. Keller, L. Mastrolorenzo, M. Merschmeyer, A. Meyer, G. Mocellin, S. Mondal, S. Mukherjee, D. Noll, A. Novak, T. Pook, A. Pozdnyakov, Y. Rath, H. Reithler, J. Roemer, A. Schmidt, S.C. Schuler, A. Sharma, S. Wiedenbeck, S. Zaleski

RWTH Aachen University, III. Physikalisches Institut A, Aachen, Germany

C. Dziwok, G. Flügge, W. Haj Ahmad¹⁹, O. Hlushchenko, T. Kress, A. Nowack, C. Pistone, O. Pooth, D. Roy, H. Sert, A. Stahl²⁰, T. Ziemons

RWTH Aachen University, III. Physikalisches Institut B, Aachen, Germany

H. Aarup Petersen, M. Aldaya Martin, P. Asmuss, I. Babounikau, S. Baxter, O. Behnke, A. Bermúdez Martínez, A.A. Bin Anuar, K. Borras²¹, V. Botta, D. Brunner, A. Campbell, A. Cardini, P. Connor, S. Consuegra Rodríguez, V. Danilov, A. De Wit, M.M. Defranchis, L. Didukh, D. Domínguez Damiani, G. Eckerlin, D. Eckstein, L.I. Estevez Banos, E. Gallo²², A. Geiser, A. Giraldi, A. Grohsjean, M. Guthoff, A. Harb, A. Jafari²³, N.Z. Jomhari, H. Jung, A. Kasem²¹, M. Kasemann, H. Kaveh, C. Kleinwort, J. Knolle, D. Krücker, W. Lange, T. Lenz, J. Lidrych, K. Lipka, W. Lohmann²⁴, T. Madlener, R. Mankel, I.-A. Melzer-Pellmann, J. Metwally, A.B. Meyer, M. Meyer, J. Mnich, A. Mussgiller, V. Myronenko, Y. Otariid, D. Pérez Adán, S.K. Pflitsch, D. Pitzl, A. Raspereza, A. Saggio, A. Saibel, M. Savitskyi, V. Scheurer, C. Schwanenberger, A. Singh, R.E. Sosa Ricardo, N. Tonon, O. Turkot, A. Vagnerini, M. Van De Klundert, R. Walsh, D. Walter, Y. Wen, K. Wichmann, C. Wissing, S. Wuchterl, O. Zenaiev, R. Zlebcik

Deutsches Elektronen-Synchrotron, Hamburg, Germany

R. Aggleton, S. Bein, L. Benato, A. Benecke, K. De Leo, T. Dreyer, M. Eich, F. Feindt, A. Fröhlich, C. Garbers, E. Garutti, P. Gunnellini, J. Haller, A. Hinzmann, A. Karavdina, G. Kasieczka, R. Klanner, R. Kogler, V. Kutzner, J. Lange, T. Lange, A. Malara, C.E.N. Niemeyer, A. Nigamova, K.J. Pena Rodriguez, O. Rieger, P. Schleper, M. Schröder, S. Schumann, J. Schwandt, D. Schwarz, J. Sonneveld, H. Stadie, G. Steinbrück, A. Tews, B. Vormwald, I. Zoi

University of Hamburg, Hamburg, Germany

J. Bechtel, T. Berger, E. Butz, R. Caspart, T. Chwalek, W. De Boer, A. Dierlamm, A. Droll, K. El Morabit, N. Faltermann, K. Flöh, M. Giffels, J.o. Gosewisch, A. Gottmann, F. Hartmann²⁰, C. Heidecker, U. Husemann, I. Katkov²⁵, P. Keicher, R. Koppenhöfer, S. Maier, M. Metzler, S. Mitra, Th. Müller, M. Musich, M. Neukum, G. Quast, K. Rabbertz, J. Rauser, D. Savoiu, D. Schäfer, M. Schnepf, D. Seith, I. Shvetsov, H.J. Simonis, R. Ulrich, J. Van Der Linden, R.F. Von Cube, M. Wassmer, M. Weber, S. Wieland, R. Wolf, S. Wozniewski, S. Wunsch

Karlsruher Institut fuer Technologie, Karlsruhe, Germany

G. Anagnostou, P. Asenov, G. Daskalakis, T. Geralis, A. Kyriakis, D. Loukas, G. Paspalaki, A. Stakia

Institute of Nuclear and Particle Physics (INPP), NCSR Demokritos, Aghia Paraskevi, Greece

M. Diamantopoulou, D. Karasavvas, G. Karathanasis, P. Kontaxakis, C.K. Koraka, A. Manousakis-Katsikakis, A. Panagiotou, I. Papavergou, N. Saoulidou, K. Theofilatos, E. Tziaferi, K. Vellidis, E. Vourliotis

National and Kapodistrian University of Athens, Athens, Greece

G. Bakas, K. Kousouris, I. Papakrivopoulos, G. Tsipolitis, A. Zacharopoulou

National Technical University of Athens, Athens, Greece

I. Evangelou, C. Foudas, P. Gianneios, P. Katsoulis, P. Kokkas, K. Manitaras, N. Manthos, I. Papadopoulos, J. Strologas

University of Ioánnina, Ioánnina, Greece

M. Csanad, M.M.A. Gadallah²⁶, S. Lökös²⁷, P. Major, K. Mandal, A. Mehta, G. Pasztor, O. Surányi, G.I. Veres

MTA-ELTE Lendület CMS Particle and Nuclear Physics Group, Eötvös Loránd University, Budapest, Hungary

M. Bartók²⁸, G. Bencze, C. Hajdu, D. Horvath²⁹, F. Sikler, V. Veszpremi, G. Vesztergombi[†]

Wigner Research Centre for Physics, Budapest, Hungary

S. Czellar, J. Karancsi²⁸, J. Molnar, Z. Szillasi, D. Teyssier

Institute of Nuclear Research ATOMKI, Debrecen, Hungary

P. Raics, Z.L. Trocsanyi³⁰, B. Ujvari

Institute of Physics, University of Debrecen, Debrecen, Hungary

T. Csorgo³¹, F. Nemes³¹, T. Novak

Eszterhazy Karoly University, Karoly Robert Campus, Gyongyos, Hungary

S. Choudhury, J.R. Komaragiri, D. Kumar, L. Panwar, P.C. Tiwari

Indian Institute of Science (IISc), Bangalore, India

S. Bahinipati³², D. Dash, C. Kar, P. Mal, T. Mishra, V.K. Muraleedharan Nair Bindhu³³, A. Nayak³³, N. Sur, S.K. Swain

National Institute of Science Education and Research, HBNI, Bhubaneswar, India

S. Bansal, S.B. Beri, V. Bhatnagar, G. Chaudhary, S. Chauhan, N. Dhingra³⁴, R. Gupta, A. Kaur, S. Kaur, P. Kumari, M. Meena, K. Sandeep, J.B. Singh, A.K. Viridi

Panjab University, Chandigarh, India

A. Ahmed, A. Bhardwaj, B.C. Choudhary, R.B. Garg, M. Gola, S. Keshri, A. Kumar, M. Naimuddin, P. Priyanka, K. Ranjan, A. Shah

University of Delhi, Delhi, India

M. Bharti³⁵, R. Bhattacharya, S. Bhattacharya, D. Bhowmik, S. Dutta, S. Ghosh, B. Gomber³⁶, M. Maity³⁷, S. Nandan, P. Palit, P.K. Rout, G. Saha, B. Sahu, S. Sarkar, M. Sharan, B. Singh³⁵, S. Thakur³⁵

Saha Institute of Nuclear Physics, HBNI, Kolkata, India

P.K. Behera, S.C. Behera, P. Kalbhor, A. Muhammad, R. Pradhan, P.R. Pujahari, A. Sharma, A.K. Sikdar

Indian Institute of Technology Madras, Madras, India

D. Dutta, V. Jha, V. Kumar, D.K. Mishra, K. Naskar³⁸, P.K. Netrakanti, L.M. Pant, P. Shukla

Bhabha Atomic Research Centre, Mumbai, India

T. Aziz, S. Dugad, G.B. Mohanty, U. Sarkar

Tata Institute of Fundamental Research-A, Mumbai, India

S. Banerjee, S. Bhattacharya, S. Chatterjee, R. Chudasama, M. Guchait, S. Karmakar, S. Kumar, G. Majumder, K. Mazumdar, S. Mukherjee, D. Roy

Tata Institute of Fundamental Research-B, Mumbai, India

S. Dube, B. Kansal, S. Pandey, A. Rane, A. Rastogi, S. Sharma

Indian Institute of Science Education and Research (IISER), Pune, India

H. Bakhshiansohi³⁹, M. Zeinali⁴⁰

Department of Physics, Isfahan University of Technology, Isfahan, Iran

S. Chenarani⁴¹, S.M. Etesami, M. Khakzad, M. Mohammadi Najafabadi

Institute for Research in Fundamental Sciences (IPM), Tehran, Iran

M. Felcini, M. Grunewald

University College Dublin, Dublin, Ireland

M. Abbrescia^{a,b}, R. Aly^{a,b,42}, C. Aruta^{a,b}, A. Colaleo^a, D. Creanza^{a,c}, N. De Filippis^{a,c}, M. De Palma^{a,b}, A. Di Florio^{a,b}, A. Di Pilato^{a,b}, W. Elmetenawee^{a,b}, L. Fiore^a, A. Gelmi^{a,b}, M. Gul^a, G. Iaselli^{a,c}, M. Ince^{a,b}, S. Lezki^{a,b}, G. Maggi^{a,c}, M. Maggi^a, I. Margjeka^{a,b}, V. Mastrapasqua^{a,b}, J.A. Merlin^a, S. My^{a,b}, S. Nuzzo^{a,b}, A. Pompili^{a,b}, G. Pugliese^{a,c}, A. Ranieri^a, G. Selvaggi^{a,b}, L. Silvestris^a, F.M. Simone^{a,b}, R. Venditti^a, P. Verwilligen^a

^a INFN Sezione di Bari, Bari, Italy

^b Università di Bari, Bari, Italy

^c Politecnico di Bari, Bari, Italy

G. Abbiendi^a, C. Battilana^{a,b}, D. Bonacorsi^{a,b}, L. Borghonovi^a, S. Braibant-Giacomelli^{a,b}, R. Campanini^{a,b}, P. Capiluppi^{a,b}, A. Castro^{a,b}, F.R. Cavallo^a, C. Ciocca^a, M. Cuffiani^{a,b}, G.M. Dallavalle^a, T. Diotallevi^{a,b}, F. Fabbri^a, A. Fanfani^{a,b}, E. Fontanesi^{a,b}, P. Giacomelli^a, L. Giommi^{a,b}, C. Grandi^a, L. Guiducci^{a,b}, F. Iemmi^{a,b}, S. Lo Meo^{a,43}, S. Marcellini^a, G. Masetti^a, F.L. Navarria^{a,b}, A. Perrotta^a, F. Primavera^{a,b}, A.M. Rossi^{a,b}, T. Rovelli^{a,b}, G.P. Siroli^{a,b}, N. Tosi^a

^a INFN Sezione di Bologna, Bologna, Italy

^b Università di Bologna, Bologna, Italy

S. Albergo ^{a,b,44}, S. Costa ^{a,b}, A. Di Mattia ^a, R. Potenza ^{a,b}, A. Tricomi ^{a,b,44}, C. Tuve ^{a,b}

^a INFN Sezione di Catania, Catania, Italy

^b Università di Catania, Catania, Italy

G. Barbagli ^a, A. Cassese ^a, R. Ceccarelli ^{a,b}, V. Ciulli ^{a,b}, C. Civinini ^a, R. D'Alessandro ^{a,b}, F. Fiori ^a,
E. Focardi ^{a,b}, G. Latino ^{a,b}, P. Lenzi ^{a,b}, M. Lizzo ^{a,b}, M. Meschini ^a, S. Paoletti ^a, R. Seidita ^{a,b},
G. Sguazzoni ^a, L. Viliani ^a

^a INFN Sezione di Firenze, Firenze, Italy

^b Università di Firenze, Firenze, Italy

L. Benussi, S. Bianco, D. Piccolo

INFN Laboratori Nazionali di Frascati, Frascati, Italy

M. Bozzo ^{a,b}, F. Ferro ^a, R. Mulargia ^{a,b}, E. Robutti ^a, S. Tosi ^{a,b}

^a INFN Sezione di Genova, Genova, Italy

^b Università di Genova, Genova, Italy

A. Benaglia ^a, A. Beschi ^{a,b}, F. Brivio ^{a,b}, F. Cetorelli ^{a,b}, V. Ciriolo ^{a,b,20}, F. De Guio ^{a,b}, M.E. Dinardo ^{a,b},
P. Dini ^a, S. Gennai ^a, A. Ghezzi ^{a,b}, P. Govoni ^{a,b}, L. Guzzi ^{a,b}, M. Malberti ^a, S. Malvezzi ^a, A. Massironi ^a,
D. Menasce ^a, F. Monti ^{a,b}, L. Moroni ^a, M. Paganoni ^{a,b}, D. Pedrini ^a, S. Ragazzi ^{a,b}, T. Tabarelli de Fatis ^{a,b},
D. Valsecchi ^{a,b,20}, D. Zuolo ^{a,b}

^a INFN Sezione di Milano-Bicocca, Milano, Italy

^b Università di Milano-Bicocca, Milano, Italy

S. Buontempo ^a, N. Cavallo ^{a,c}, A. De Iorio ^{a,b}, F. Fabozzi ^{a,c}, F. Fienga ^a, A.O.M. Iorio ^{a,b}, L. Lista ^{a,b},
S. Meola ^{a,d,20}, P. Paolucci ^{a,20}, B. Rossi ^a, C. Sciacca ^{a,b}

^a INFN Sezione di Napoli, Napoli, Italy

^b Università di Napoli "Federico II", Napoli, Italy

^c Università della Basilicata, Potenza, Italy

^d Università G. Marconi, Roma, Italy

P. Azzi ^a, N. Bacchetta ^a, D. Bisello ^{a,b}, P. Bortignon ^a, A. Bragagnolo ^{a,b}, R. Carlin ^{a,b}, P. Checchia ^a,
P. De Castro Manzano ^a, T. Dorigo ^a, F. Gasparini ^{a,b}, U. Gasparini ^{a,b}, S.Y. Hoh ^{a,b}, L. Layer ^{a,45},
M. Margoni ^{a,b}, A.T. Meneguzzo ^{a,b}, M. Presilla ^{a,b}, P. Ronchese ^{a,b}, R. Rossin ^{a,b}, F. Simonetto ^{a,b},
G. Strong ^a, M. Tosi ^{a,b}, H. Yarar ^{a,b}, M. Zanetti ^{a,b}, P. Zotto ^{a,b}, A. Zucchetta ^{a,b}, G. Zumerle ^{a,b}

^a INFN Sezione di Padova, Padova, Italy

^b Università di Padova, Padova, Italy

^c Università di Trento, Trento, Italy

C. Aime ^{a,b}, A. Braghieri ^a, S. Calzaferri ^{a,b}, D. Fiorina ^{a,b}, P. Montagna ^{a,b}, S.P. Ratti ^{a,b}, V. Re ^a,
M. Ressegotti ^{a,b}, C. Riccardi ^{a,b}, P. Salvini ^a, I. Vai ^a, P. Vitulo ^{a,b}

^a INFN Sezione di Pavia, Pavia, Italy

^b Università di Pavia, Pavia, Italy

G.M. Bilei ^a, D. Ciangottini ^{a,b}, L. Fanò ^{a,b}, P. Lariccia ^{a,b}, G. Mantovani ^{a,b}, V. Mariani ^{a,b}, M. Menichelli ^a,
F. Moscatelli ^a, A. Piccinelli ^{a,b}, A. Rossi ^{a,b}, A. Santocchia ^{a,b}, D. Spiga ^a, T. Tedeschi ^{a,b}

^a INFN Sezione di Perugia, Perugia, Italy

^b Università di Perugia, Perugia, Italy

K. Androsov ^a, P. Azzurri ^a, G. Bagliesi ^a, V. Bertacchi ^{a,c}, L. Bianchini ^a, T. Boccali ^a, E. Bossini, R. Castaldi ^a,
M.A. Ciocci ^{a,b}, R. Dell'Orso ^a, M.R. Di Domenico ^{a,d}, S. Donato ^a, A. Giassi ^a, M.T. Grippo ^a, F. Ligabue ^{a,c},
E. Manca ^{a,c}, G. Mandorli ^{a,c}, A. Messineo ^{a,b}, F. Palla ^a, G. Ramirez-Sanchez ^{a,c}, A. Rizzi ^{a,b}, G. Rolandi ^{a,c},
S. Roy Chowdhury ^{a,c}, A. Scribano ^a, N. Shafiei ^{a,b}, P. Spagnolo ^a, R. Tenchini ^a, G. Tonelli ^{a,b}, N. Turini ^{a,d},
A. Venturi ^a, P.G. Verdini ^a

^a INFN Sezione di Pisa, Pisa Italy

^b Università di Pisa, Pisa Italy

^c Scuola Normale Superiore di Pisa, Pisa Italy^d Università di Siena, Siena, Italy

F. Cavallari ^a, M. Cipriani ^{a,b}, D. Del Re ^{a,b}, E. Di Marco ^a, M. Diemoz ^a, E. Longo ^{a,b}, P. Meridiani ^a,
 G. Organtini ^{a,b}, F. Pandolfi ^a, R. Paramatti ^{a,b}, C. Quaranta ^{a,b}, S. Rahatlou ^{a,b}, C. Rovelli ^a,
 F. Santanastasio ^{a,b}, L. Soffi ^{a,b}, R. Tramontano ^{a,b}

^a INFN Sezione di Roma, Rome, Italy^b Sapienza Università di Roma, Rome, Italy

N. Amapane ^{a,b}, R. Arcidiacono ^{a,c}, S. Argiro ^{a,b}, M. Arneodo ^{a,c}, N. Bartosik ^a, R. Bellan ^{a,b}, A. Bellora ^{a,b},
 J. Berenguer Antequera ^{a,b}, C. Biino ^a, A. Cappati ^{a,b}, N. Cartiglia ^a, S. Cometti ^a, M. Costa ^{a,b},
 R. Covarelli ^{a,b}, N. Demaria ^a, B. Kiani ^{a,b}, F. Legger ^a, C. Mariotti ^a, S. Maselli ^a, E. Migliore ^{a,b},
 V. Monaco ^{a,b}, E. Monteil ^{a,b}, M. Monteno ^a, M.M. Obertino ^{a,b}, G. Ortona ^a, L. Pacher ^{a,b}, N. Pastrone ^a,
 M. Pelliccioni ^a, G.L. Pinna Angioni ^{a,b}, M. Ruspa ^{a,c}, R. Salvatico ^{a,b}, F. Siviero ^{a,b}, V. Sola ^a, A. Solano ^{a,b},
 D. Soldi ^{a,b}, A. Staiano ^a, M. Tornago ^{a,b}, D. Trocino ^{a,b}

^a INFN Sezione di Torino, Torino, Italy^b Università di Torino, Torino, Italy^c Università del Piemonte Orientale, Novara, Italy

S. Belforte ^a, V. Candelise ^{a,b}, M. Casarsa ^a, F. Cossutti ^a, A. Da Rold ^{a,b}, G. Della Ricca ^{a,b}, F. Vazzoler ^{a,b}

^a INFN Sezione di Trieste, Trieste, Italy^b Università di Trieste, Trieste, Italy

S. Dogra, C. Huh, B. Kim, D.H. Kim, G.N. Kim, J. Lee, S.W. Lee, C.S. Moon, Y.D. Oh, S.I. Pak,
 B.C. Radburn-Smith, S. Sekmen, Y.C. Yang

Kyungpook National University, Daegu, Republic of Korea

H. Kim, D.H. Moon

Chonnam National University, Institute for Universe and Elementary Particles, Kwangju, Republic of Korea

B. Francois, T.J. Kim, J. Park

Hanyang University, Seoul, Republic of Korea

S. Cho, S. Choi, Y. Go, B. Hong, K. Lee, K.S. Lee, J. Lim, J. Park, S.K. Park, J. Yoo

Korea University, Seoul, Republic of Korea

J. Goh, A. Gurtu

Kyung Hee University, Department of Physics, Seoul, Republic of Korea

H.S. Kim, Y. Kim

Sejong University, Seoul, Republic of Korea

J. Almond, J.H. Bhyun, J. Choi, S. Jeon, J. Kim, J.S. Kim, S. Ko, H. Kwon, H. Lee, S. Lee, K. Nam, B.H. Oh,
 M. Oh, S.B. Oh, H. Seo, U.K. Yang, I. Yoon

Seoul National University, Seoul, Republic of Korea

D. Jeon, J.H. Kim, B. Ko, J.S.H. Lee, I.C. Park, Y. Roh, D. Song, I.J. Watson

University of Seoul, Seoul, Republic of Korea

S. Ha, H.D. Yoo

Yonsei University, Department of Physics, Seoul, Republic of Korea

Y. Choi, C. Hwang, Y. Jeong, H. Lee, Y. Lee, I. Yu

Sungkyunkwan University, Suwon, Republic of Korea

Y. Maghrbi

College of Engineering and Technology, American University of the Middle East (AUM), Dasman, Kuwait

V. Veckalns⁴⁶

Riga Technical University, Riga, Latvia

M. Ambrozas, A. Juodagalvis, A. Rinkevicius, G. Tamulaitis, A. Vaitkevicius

Vilnius University, Vilnius, Lithuania

W.A.T. Wan Abdullah, M.N. Yusli, Z. Zolkapli

National Centre for Particle Physics, Universiti Malaya, Kuala Lumpur, Malaysia

J.F. Benitez, A. Castaneda Hernandez, J.A. Murillo Quijada, L. Valencia Palomo

Universidad de Sonora (UNISON), Hermosillo, Mexico

G. Ayala, H. Castilla-Valdez, E. De La Cruz-Burelo, I. Heredia-De La Cruz⁴⁷, R. Lopez-Fernandez, C.A. Mondragon Herrera, D.A. Perez Navarro, A. Sanchez-Hernandez

Centro de Investigacion y de Estudios Avanzados del IPN, Mexico City, Mexico

S. Carrillo Moreno, C. Oropeza Barrera, M. Ramirez-Garcia, F. Vazquez Valencia

Universidad Iberoamericana, Mexico City, Mexico

I. Pedraza, H.A. Salazar Ibarquen, C. Uribe Estrada

Benemerita Universidad Autonoma de Puebla, Puebla, Mexico

J. Mijuskovic⁴, N. Raicevic

University of Montenegro, Podgorica, Montenegro

D. Krofcheck

University of Auckland, Auckland, New Zealand

S. Bheesette, P.H. Butler

University of Canterbury, Christchurch, New Zealand

A. Ahmad, M.I. Asghar, A. Awais, M.I.M. Awan, H.R. Hoorani, W.A. Khan, M.A. Shah, M. Shoib, M. Waqas

National Centre for Physics, Quaid-I-Azam University, Islamabad, Pakistan

V. Avati, L. Grzanka, M. Malawski

AGH University of Science and Technology Faculty of Computer Science, Electronics and Telecommunications, Krakow, Poland

H. Bialkowska, M. Bluj, B. Boimska, T. Frueboes, M. Górski, M. Kazana, M. Szleper, P. Traczyk, P. Zalewski

National Centre for Nuclear Research, Swierk, Poland

K. Bunkowski, K. Doroba, A. Kalinowski, M. Konecki, J. Krolikowski, M. Walczak

Institute of Experimental Physics, Faculty of Physics, University of Warsaw, Warsaw, Poland

M. Araujo, P. Bargassa, D. Bastos, A. Boletti, P. Faccioli, M. Gallinaro, J. Hollar, N. Leonardo, T. Niknejad, J. Seixas, K. Shchelina, O. Toldaiev, J. Varela

Laboratório de Instrumentação e Física Experimental de Partículas, Lisboa, Portugal

S. Afanasiev, D. Budkouski, P. Bunin, M. Gavrilenko, I. Golutvin, I. Gorbunov, A. Kamenev, V. Karjavine, A. Lanev, A. Malakhov, V. Matveev^{48,49}, V. Palichik, V. Perelygin, M. Savina, D. Seitova, V. Shalaev, S. Shmatov, S. Shulha, V. Smirnov, O. Teryaev, N. Voytishin, A. Zarubin, I. Zhizhin

Joint Institute for Nuclear Research, Dubna, Russia

G. Gavrillov, V. Golovtsov, Y. Ivanov, V. Kim⁵⁰, E. Kuznetsova⁵¹, V. Murzin, V. Oreshkin, I. Smirnov, D. Sosnov, V. Sulimov, L. Uvarov, S. Volkov, A. Vorobyev

Petersburg Nuclear Physics Institute, Gatchina (St. Petersburg), Russia

Yu. Andreev, A. Dermenev, S. Gninenko, N. Golubev, A. Karneyeu, M. Kirsanov, N. Krasnikov, A. Pashenkov, G. Pivovarov, D. Tlisov[†], A. Toropin

Institute for Nuclear Research, Moscow, Russia

V. Epshteyn, V. Gavrillov, N. Lychkovskaya, A. Nikitenko⁵², V. Popov, G. Safronov, A. Spiridonov, A. Steppenov, M. Toms, E. Vlasov, A. Zhokin

Institute for Theoretical and Experimental Physics named by A.I. Alikhanov of NRC 'Kurchatov Institute', Moscow, Russia

T. Aushev

Moscow Institute of Physics and Technology, Moscow, Russia

R. Chistov⁵³, M. Danilov⁵⁴, A. Oskin, P. Parygin, S. Polikarpov⁵³

National Research Nuclear University 'Moscow Engineering Physics Institute' (MEPhI), Moscow, Russia

V. Andreev, M. Azarkin, I. Dremin, M. Kirakosyan, A. Terkulov

P.N. Lebedev Physical Institute, Moscow, Russia

A. Belyaev, E. Boos, V. Bunichev, M. Dubinin⁵⁵, L. Dudko, A. Gribushin, V. Klyukhin, N. Korneeva, I. Lokhtin, S. Obraztsov, M. Perfilov, V. Savrin, P. Volkov

Skobeltsyn Institute of Nuclear Physics, Lomonosov Moscow State University, Moscow, Russia

V. Blinov⁵⁶, T. Dimova⁵⁶, L. Kardapoltsev⁵⁶, I. Ovtin⁵⁶, Y. Skovpen⁵⁶

Novosibirsk State University (NSU), Novosibirsk, Russia

I. Azhgirey, I. Bayshev, V. Kachanov, A. Kalinin, D. Konstantinov, V. Petrov, R. Ryutin, A. Sobol, S. Troshin, N. Tyurin, A. Uzunian, A. Volkov

Institute for High Energy Physics of National Research Centre 'Kurchatov Institute', Protvino, Russia

A. Babaev, A. Iuzhakov, V. Okhotnikov, L. Sukhikh

National Research Tomsk Polytechnic University, Tomsk, Russia

V. Borchsh, V. Ivanchenko, E. Tcherniaev

Tomsk State University, Tomsk, Russia

P. Adzic⁵⁷, M. Dordevic, P. Milenovic, J. Milosevic

University of Belgrade: Faculty of Physics and VINCA Institute of Nuclear Sciences, Belgrade, Serbia

M. Aguilar-Benitez, J. Alcaraz Maestre, A. Álvarez Fernández, I. Bachiller, M. Barrio Luna, Cristina F. Bedoya, C.A. Carrillo Montoya, M. Cepeda, M. Cerrada, N. Colino, B. De La Cruz, A. Delgado Peris, J.P. Fernández Ramos, J. Flix, M.C. Fouz, O. Gonzalez Lopez, S. Goy Lopez, J.M. Hernandez, M.I. Josa, J. León Holgado, D. Moran, Á. Navarro Tobar, A. Pérez-Calero Yzquierdo, J. Puerta Pelayo, I. Redondo, L. Romero, S. Sánchez Navas, M.S. Soares, L. Urda Gómez, C. Willmott

Centro de Investigaciones Energéticas Medioambientales y Tecnológicas (CIEMAT), Madrid, Spain

C. Albajar, J.F. de Trocóniz, R. Reyes-Almanza

Universidad Autónoma de Madrid, Madrid, Spain

B. Alvarez Gonzalez, J. Cuevas, C. Erice, J. Fernandez Menendez, S. Folgueras, I. Gonzalez Caballero, E. Palencia Cortezon, C. Ramón Álvarez, J. Ripoll Sau, V. Rodríguez Bouza, S. Sanchez Cruz, A. Trapote

Universidad de Oviedo, Instituto Universitario de Ciencias y Tecnologías Espaciales de Asturias (ICTEA), Oviedo, Spain

J.A. Brochero Cifuentes, I.J. Cabrillo, A. Calderon, B. Chazin Quero, J. Duarte Campderros, M. Fernandez, C. Fernandez Madrazo, P.J. Fernández Manteca, A. García Alonso, G. Gomez, C. Martinez Rivero, P. Martinez Ruiz del Arbol, F. Matorras, J. Piedra Gomez, C. Prieels, F. Ricci-Tam, T. Rodrigo, A. Ruiz-Jimeno, L. Scodellaro, N. Trevisani, I. Vila, J.M. Vizan Garcia

Instituto de Física de Cantabria (IFCA), CSIC-Universidad de Cantabria, Santander, Spain

M.K. Jayananda, B. Kailasapathy⁵⁸, D.U.J. Sonnadara, D.D.C. Wickramaratna

University of Colombo, Colombo, Sri Lanka

W.G.D. Dharmaratna, K. Liyanage, N. Perera, N. Wickramage

University of Ruhuna, Department of Physics, Matara, Sri Lanka

T.K. Aarrestad, D. Abbaneo, E. Auffray, G. Auzinger, J. Baechler, P. Baillon, A.H. Ball, D. Barney, J. Bendavid, N. Beni, M. Bianco, A. Bocci, E. Brondolin, T. Camporesi, M. Capeans Garrido, G. Cerminara, S.S. Chhibra, L. Cristella, D. d'Enterria, A. Dabrowski, N. Daci, A. David, A. De Roeck, M. Deile, R. Di Maria, M. Dobson, M. Dünser, N. Dupont, A. Elliott-Peisert, N. Emriskova, F. Fallavollita⁵⁹, D. Fasanella, S. Fiorendi, A. Florent, G. Franzoni, J. Fulcher, W. Funk, S. Giani, D. Gigi, K. Gill, F. Glege, L. Gouskos, M. Guilbaud, M. Haranko, J. Hegeman, Y. Iiyama, V. Innocente, T. James, P. Janot, J. Kaspar, J. Kieseler, M. Komm, N. Kratochwil, C. Lange, S. Laurila, P. Lecoq, K. Long, C. Lourenço, L. Malgeri, S. Mallios, M. Mannelli, F. Meijers, S. Mersi, E. Meschi, F. Moortgat, M. Mulders, S. Orfanelli, L. Orsini, F. Pantaleo²⁰, L. Pape, E. Perez, M. Peruzzi, A. Petrilli, G. Petrucciani, A. Pfeiffer, M. Pierini, T. Quast, D. Rabady, A. Racz, M. Rieger, M. Rovere, H. Sakulin, J. Salfeld-Nebgen, S. Scarfi, C. Schäfer, C. Schwick, M. Selvaggi, A. Sharma, P. Silva, W. Snoeys, P. Sphicas⁶⁰, S. Summers, V.R. Tavolaro, D. Treille, A. Tsiros, G.P. Van Onsem, M. Verzetti, K.A. Wozniak, W.D. Zeuner

CERN, European Organization for Nuclear Research, Geneva, Switzerland

L. Caminada⁶¹, A. Ebrahimi, W. Erdmann, R. Horisberger, Q. Ingram, H.C. Kaestli, D. Kotlinski, U. Langenegger, M. Missiroli, T. Rohe

Paul Scherrer Institut, Villigen, Switzerland

M. Backhaus, P. Berger, A. Calandri, N. Chernyavskaya, A. De Cosa, G. Dissertori, M. Dittmar, M. Donegà, C. Dorfer, T. Gadek, T.A. Gómez Espinosa, C. Grab, D. Hits, W. Lustermann, A.-M. Lyon, R.A. Manzoni, M.T. Meinhard, F. Micheli, F. Nessi-Tedaldi, J. Niedziela, F. Pauss, V. Perovic, G. Perrin, S. Pigazzini, M.G. Ratti, M. Reichmann, C. Reissel, T. Reitenspiess, B. Ristic, D. Ruini, D.A. Sanz Becerra, M. Schönenberger, V. Stampf, J. Steggemann⁶², R. Wallny, D.H. Zhu

ETH Zurich – Institute for Particle Physics and Astrophysics (IPA), Zurich, Switzerland

C. Amsler⁶³, C. Botta, D. Brzhechko, M.F. Canelli, R. Del Burgo, J.K. Heikkilä, M. Huwiler, A. Jofrehei, B. Kilminster, S. Leontsinis, A. Macchiolo, P. Meiring, V.M. Mikuni, U. Molinatti, I. Neutelings, G. Rauco, A. Reimers, P. Robmann, K. Schweiger, Y. Takahashi

Universität Zürich, Zurich, Switzerland

C. Adloff⁶⁴, C.M. Kuo, W. Lin, A. Roy, T. Sarkar³⁷, S.S. Yu

National Central University, Chung-Li, Taiwan

L. Ceard, P. Chang, Y. Chao, K.F. Chen, P.H. Chen, W.-S. Hou, Y.y. Li, R.-S. Lu, E. Paganis, A. Psallidas, A. Steen, E. Yazgan

National Taiwan University (NTU), Taipei, Taiwan

B. Asavapibhop, C. Asawatangtrakuldee, N. Srimanobhas

Chulalongkorn University, Faculty of Science, Department of Physics, Bangkok, Thailand

F. Boran, S. Damarseekin⁶⁵, Z.S. Demiroglu, F. Dolek, C. Dozen⁶⁶, I. Dumanoglu⁶⁷, E. Eskut, G. Gokbulut, Y. Guler, E. Gurpinar Guler⁶⁸, I. Hos⁶⁹, C. Isik, E.E. Kangal⁷⁰, O. Kara, A. Kayis Topaksu, U. Kiminsu, G. Onengut, K. Ozdemir⁷¹, A. Polatoz, A.E. Simsek, B. Tali⁷², U.G. Tok, S. Turkcapar, I.S. Zorbakir, C. Zorbilmez

Çukurova University, Physics Department, Science and Art Faculty, Adana, Turkey

B. Isildak⁷³, G. Karapinar⁷⁴, K. Ocalan⁷⁵, M. Yalvac⁷⁶

Middle East Technical University, Physics Department, Ankara, Turkey

B. Akgun, I.O. Atakisi, E. Gülmez, M. Kaya⁷⁷, O. Kaya⁷⁸, Ö. Özçelik, S. Tekten⁷⁹, E.A. Yetkin⁸⁰

Bogazici University, Istanbul, Turkey

A. Cakir, K. Cankocak⁶⁷, Y. Komurcu, S. Sen⁸¹

Istanbul Technical University, Istanbul, Turkey

F. Aydogmus Sen, S. Cerci⁷², B. Kaynak, S. Ozkorucuklu, D. Sunar Cerci⁷²

Istanbul University, Istanbul, Turkey

B. Grynyov

Institute for Scintillation Materials of National Academy of Science of Ukraine, Kharkov, Ukraine

L. Levchuk

National Scientific Center, Kharkov Institute of Physics and Technology, Kharkov, Ukraine

E. Bhal, S. Bologna, J.J. Brooke, A. Bundock, E. Clement, D. Cussans, H. Flacher, J. Goldstein, G.P. Heath, H.F. Heath, L. Kreczko, B. Krikler, S. Paramesvaran, T. Sakuma, S. Seif El Nasr-Storey, V.J. Smith, N. Stylianou⁸², J. Taylor, A. Titterton

University of Bristol, Bristol, United Kingdom

K.W. Bell, A. Belyaev⁸³, C. Brew, R.M. Brown, D.J.A. Cockerill, K.V. Ellis, K. Harder, S. Harper, J. Linacre, K. Manolopoulos, D.M. Newbold, E. Olaiya, D. Petyt, T. Reis, T. Schuh, C.H. Shepherd-Themistocleous, A. Thea, I.R. Tomalin, T. Williams

Rutherford Appleton Laboratory, Didcot, United Kingdom

R. Bainbridge, P. Bloch, S. Bonomally, J. Borg, S. Breeze, O. Buchmuller, V. Cepaitis, G.S. Chahal⁸⁴, D. Colling, P. Dauncey, G. Davies, M. Della Negra, G. Fedi, G. Hall, G. Iles, J. Langford, L. Lyons, A.-M. Magnan, S. Malik, A. Martelli, V. Milosevic, J. Nash⁸⁵, V. Palladino, M. Pesaresi, D.M. Raymond, A. Richards, A. Rose, E. Scott, C. Seez, A. Shtipliyski, A. Tapper, K. Uchida, T. Virdee²⁰, N. Wardle, S.N. Webb, D. Winterbottom, A.G. Zecchinelli

Imperial College, London, United Kingdom

J.E. Cole, A. Khan, P. Kyberd, C.K. Mackay, I.D. Reid, L. Teodorescu, S. Zahid

Brunel University, Uxbridge, United Kingdom

S. Abdullin, A. Brinkerhoff, K. Call, B. Caraway, J. Dittmann, K. Hatakeyama, A.R. Kanuganti, C. Madrid, B. McMaster, N. Pastika, S. Sawant, C. Smith, C. Sutantawibul, J. Wilson

Baylor University, Waco, USA

R. Bartek, A. Dominguez, R. Uniyal, A.M. Vargas Hernandez

Catholic University of America, Washington, DC, USA

A. Buccilli, O. Charaf, S.I. Cooper, D. Di Croce, S.V. Gleyzer, C. Henderson, C.U. Perez, P. Rumerio, C. West

The University of Alabama, Tuscaloosa, USA

A. Akpinar, A. Albert, D. Arcaro, C. Cosby, Z. Demiragli, D. Gastler, J. Rohlf, K. Salyer, D. Sperka, D. Spitzbart, I. Suarez, S. Yuan, D. Zou

Boston University, Boston, USA

G. Benelli, B. Burkle, X. Coubez²¹, D. Cutts, Y.t. Duh, M. Hadley, U. Heintz, J.M. Hogan⁸⁶, K.H.M. Kwok, E. Laird, G. Landsberg, K.T. Lau, J. Lee, J. Luo, M. Narain, S. Sagir⁸⁷, E. Usai, W.Y. Wong, X. Yan, D. Yu, W. Zhang

Brown University, Providence, USA

R. Band, C. Brainerd, R. Breedon, M. Calderon De La Barca Sanchez, M. Chertok, J. Conway, R. Conway, P.T. Cox, R. Erbacher, C. Flores, F. Jensen, O. Kukral, R. Lander, M. Mulhearn, D. Pellett, M. Shi, D. Taylor, M. Tripathi, Y. Yao, F. Zhang

University of California, Davis, Davis, USA

M. Bachtis, R. Cousins, A. Dasgupta, A. Datta, D. Hamilton, J. Hauser, M. Ignatenko, M.A. Iqbal, T. Lam, N. Mccoll, W.A. Nash, S. Regnard, D. Saltzberg, C. Schnaible, B. Stone, V. Valuev

University of California, Los Angeles, USA

K. Burt, Y. Chen, R. Clare, J.W. Gary, G. Hanson, G. Karapostoli, O.R. Long, N. Manganeli, M. Olmedo Negrete, W. Si, S. Wimpenny, Y. Zhang

University of California, Riverside, Riverside, USA

J.G. Branson, P. Chang, S. Cittolin, S. Cooperstein, N. Deelen, J. Duarte, R. Gerosa, L. Giannini, D. Gilbert, V. Krutelyov, J. Letts, M. Masciovecchio, S. May, S. Padhi, M. Pieri, V. Sharma, M. Tadel, A. Vartak, F. Würthwein, A. Yagil

University of California, San Diego, La Jolla, USA

N. Amin, C. Campagnari, M. Citron, A. Dorsett, V. Dutta, J. Incandela, M. Kilpatrick, B. Marsh, H. Mei, A. Ovcharova, H. Qu, M. Quinnan, J. Richman, U. Sarica, D. Stuart, S. Wang

University of California, Santa Barbara – Department of Physics, Santa Barbara, USA

A. Bornheim, O. Cerri, I. Dutta, J.M. Lawhorn, N. Lu, J. Mao, H.B. Newman, J. Ngadiuba, T.Q. Nguyen, M. Spiropulu, J.R. Vlimant, C. Wang, S. Xie, Z. Zhang, R.Y. Zhu

California Institute of Technology, Pasadena, USA

J. Alison, M.B. Andrews, T. Ferguson, T. Mudholkar, M. Paulini, I. Vorobiev

Carnegie Mellon University, Pittsburgh, USA

J.P. Cumalat, W.T. Ford, E. MacDonald, R. Patel, A. Perloff, K. Stenson, K.A. Ulmer, S.R. Wagner

University of Colorado Boulder, Boulder, USA

J. Alexander, Y. Cheng, J. Chu, D.J. Cranshaw, K. Mcdermott, J. Monroy, J.R. Patterson, D. Quach, A. Ryd, W. Sun, S.M. Tan, Z. Tao, J. Thom, P. Wittich, M. Zientek

Cornell University, Ithaca, USA

M. Albrow, M. Alyari, G. Apollinari, A. Apresyan, A. Apyan, S. Banerjee, L.A.T. Bauerdick, A. Beretvas, D. Berry, J. Berryhill, P.C. Bhat, K. Burkett, J.N. Butler, A. Canepa, G.B. Cerati, H.W.K. Cheung, F. Chlebana, M. Cremonesi, K.F. Di Petrillo, V.D. Elvira, J. Freeman, Z. Gecse, L. Gray, D. Green, S. Grünendahl, O. Gutsche, R.M. Harris, R. Heller, T.C. Herwig, J. Hirschauer, B. Jayatilaka, S. Jindariani, M. Johnson, U. Joshi, P. Klabbers, T. Klijsma, B. Klima, M.J. Kortelainen, S. Lammel, D. Lincoln, R. Lipton, T. Liu, J. Lykken, K. Maeshima, D. Mason, P. McBride, P. Merkel, S. Mrenna, S. Nahn, V. O'Dell, V. Papadimitriou, K. Pedro, C. Pena⁵⁵, O. Prokofyev, F. Ravera, A. Reinsvold Hall, L. Ristori, B. Schneider, E. Sexton-Kennedy, N. Smith, A. Soha, L. Spiegel, S. Stoynev, J. Strait, L. Taylor, S. Tkaczyk, N.V. Tran, L. Uplegger, E.W. Vaandering, H.A. Weber

Fermi National Accelerator Laboratory, Batavia, USA

D. Acosta, P. Avery, D. Bourilkov, L. Cadamuro, V. Cherepanov, F. Errico, R.D. Field, D. Guerrero, B.M. Joshi, M. Kim, J. Konigsberg, A. Korytov, K.H. Lo, K. Matchev, N. Menendez, G. Mitselmakher, D. Rosenzweig, K. Shi, J. Sturdy, J. Wang, X. Zuo

University of Florida, Gainesville, USA

T. Adams, A. Askew, D. Diaz, R. Habibullah, S. Hagopian, V. Hagopian, K.F. Johnson, R. Khurana, T. Kolberg, G. Martinez, H. Prosper, C. Schiber, R. Yohay, J. Zhang

Florida State University, Tallahassee, USA

M.M. Baarmand, S. Butalla, T. Elkafrawy¹⁵, M. Hohlmann, R. Kumar Verma, D. Noonan, M. Rahmani, M. Saunders, F. Yumiceva

Florida Institute of Technology, Melbourne, USA

M.R. Adams, L. Apanasevich, H. Becerril Gonzalez, R. Cavanaugh, X. Chen, S. Dittmer, O. Evdokimov, C.E. Gerber, D.A. Hangal, D.J. Hofman, C. Mills, G. Oh, T. Roy, M.B. Tonjes, N. Varelas, J. Viinikainen, X. Wang, Z. Wu, Z. Ye

University of Illinois at Chicago (UIC), Chicago, USA

M. Alhusseini, K. Dilsiz⁸⁸, S. Durgut, R.P. Gandrajula, M. Haytmyradov, V. Khristenko, O.K. Köseyan, J.-P. Merlo, A. Mestvirishvili⁸⁹, A. Moeller, J. Nachtman, H. Ogul⁹⁰, Y. Onel, F. Ozok⁹¹, A. Penzo, C. Snyder, E. Tiras⁹², J. Wetzel

The University of Iowa, Iowa City, USA

O. Amram, B. Blumenfeld, L. Corcodilos, M. Eminizer, A.V. Gritsan, S. Kyriacou, P. Maksimovic, C. Mantilla, J. Roskes, M. Swartz, T.Á. Vámi

Johns Hopkins University, Baltimore, USA

C. Baldenegro Barrera, P. Baringer, A. Bean, A. Bylinkin, T. Isidori, S. Khalil, J. King, G. Krintiras, A. Kropivnitskaya, C. Lindsey, N. Minafra, M. Murray, C. Rogan, C. Royon, S. Sanders, E. Schmitz, J.D. Tapia Takaki, Q. Wang, J. Williams, G. Wilson

The University of Kansas, Lawrence, USA

S. Duric, A. Ivanov, K. Kaadze, D. Kim, Y. Maravin, T. Mitchell, A. Modak

Kansas State University, Manhattan, USA

F. Rebassoo, D. Wright

Lawrence Livermore National Laboratory, Livermore, USA

E. Adams, A. Baden, O. Baron, A. Belloni, S.C. Eno, Y. Feng, N.J. Hadley, S. Jabeen, R.G. Kellogg, T. Koeth, A.C. Mignerey, S. Nabili, M. Seidel, A. Skuja, S.C. Tonwar, L. Wang, K. Wong

University of Maryland, College Park, USA

D. Abercrombie, R. Bi, S. Brandt, W. Busza, I.A. Cali, Y. Chen, M. D'Alfonso, G. Gomez Ceballos, M. Goncharov, P. Harris, M. Hu, M. Klute, D. Kovalskyi, J. Krupa, Y.-J. Lee, P.D. Luckey, B. Maier, A.C. Marini, C. Mironov, X. Niu, C. Paus, D. Rankin, C. Roland, G. Roland, Z. Shi, G.S.F. Stephans, K. Tatar, D. Velicanu, J. Wang, T.W. Wang, Z. Wang, B. Wyslouch

Massachusetts Institute of Technology, Cambridge, USA

R.M. Chatterjee, A. Evans, P. Hansen, J. Hiltbrand, Sh. Jain, M. Krohn, Y. Kubota, Z. Lesko, J. Mans, M. Revering, R. Rusack, R. Saradhy, N. Schroeder, N. Strobbe, M.A. Wadud

University of Minnesota, Minneapolis, USA

J.G. Acosta, S. Oliveros

University of Mississippi, Oxford, USA

K. Bloom, M. Bryson, S. Chauhan, D.R. Claes, C. Fangmeier, L. Finco, F. Golf, J.R. González Fernández, C. Joo, I. Kravchenko, J.E. Siado, G.R. Snow[†], W. Tabb, F. Yan

University of Nebraska-Lincoln, Lincoln, USA

G. Agarwal, H. Bandyopadhyay, L. Hay, I. Iashvili, A. Kharchilava, C. McLean, D. Nguyen, J. Pekkanen, S. Rappoccio

State University of New York at Buffalo, Buffalo, USA

G. Alverson, E. Barberis, C. Freer, Y. Haddad, A. Hortiangtham, J. Li, G. Madigan, B. Marzocchi, D.M. Morse, V. Nguyen, T. Orimoto, A. Parker, L. Skinnari, A. Tishelman-Charny, T. Wamorkar, B. Wang, A. Wisecarver, D. Wood

Northeastern University, Boston, USA

S. Bhattacharya, J. Bueghly, Z. Chen, A. Gilbert, T. Gunter, K.A. Hahn, N. Odell, M.H. Schmitt, K. Sung, M. Velasco

Northwestern University, Evanston, USA

R. Bucci, N. Dev, R. Goldouzian, M. Hildreth, K. Hurtado Anampa, C. Jessop, K. Lannon, N. Loukas, N. Marinelli, I. Mcalister, F. Meng, K. Mohrman, Y. Musienko⁴⁸, R. Ruchti, P. Siddireddy, M. Wayne, A. Wightman, M. Wolf, L. Zygala

University of Notre Dame, Notre Dame, USA

J. Alimena, B. Bylsma, B. Cardwell, L.S. Durkin, B. Francis, C. Hill, A. Lefeld, B.L. Winer, B.R. Yates

The Ohio State University, Columbus, USA

F.M. Addesa, B. Bonham, P. Das, G. Dezoort, P. Elmer, A. Frankenthal, B. Greenberg, N. Haubrich, S. Higginbotham, A. Kalogeropoulos, G. Kopp, S. Kwan, D. Lange, M.T. Lucchini, D. Marlow, K. Mei, I. Ojalvo, J. Olsen, C. Palmer, D. Stickland, C. Tully

Princeton University, Princeton, USA

S. Malik, S. Norberg

University of Puerto Rico, Mayaguez, USA

A.S. Bakshi, V.E. Barnes, R. Chawla, S. Das, L. Gutay, M. Jones, A.W. Jung, S. Karmarkar, M. Liu, G. Negro, N. Neumeister, C.C. Peng, S. Piperov, A. Purohit, J.F. Schulte, M. Stojanovic¹⁷, J. Thieman, F. Wang, R. Xiao, W. Xie

Purdue University, West Lafayette, USA

J. Dolen, N. Parashar

Purdue University Northwest, Hammond, USA

A. Baty, S. Dildick, K.M. Ecklund, S. Freed, F.J.M. Geurts, A. Kumar, W. Li, B.P. Padley, R. Redjimi, J. Roberts[†], W. Shi, A.G. Stahl Leiton

Rice University, Houston, USA

A. Bodek, P. de Barbaro, R. Demina, J.L. Dulemba, C. Fallon, T. Ferbel, M. Galanti, A. Garcia-Bellido, O. Hindrichs, A. Khukhunaishvili, E. Ranken, R. Taus

University of Rochester, Rochester, USA

B. Chiarito, J.P. Chou, A. Gandrakota, Y. Gershtein, E. Halkiadakis, A. Hart, M. Heindl, E. Hughes, S. Kaplan, O. Karacheban²⁴, I. Laflotte, A. Lath, R. Montalvo, K. Nash, M. Osherson, S. Salur, S. Schnetzer, S. Somalwar, R. Stone, S.A. Thayil, S. Thomas, H. Wang

Rutgers, The State University of New Jersey, Piscataway, USA

H. Acharya, A.G. Delannoy, S. Spanier

University of Tennessee, Knoxville, USA

O. Bouhali⁹³, M. Dalchenko, A. Delgado, R. Eusebi, J. Gilmore, T. Huang, T. Kamon⁹⁴, H. Kim, S. Luo, S. Malhotra, R. Mueller, D. Overton, D. Rathjens, A. Safonov

Texas A&M University, College Station, USA

N. Akchurin, J. Damgov, V. Hegde, S. Kunori, K. Lamichhane, S.W. Lee, T. Mengke, S. Muthumuni, T. Peltola, S. Undleeb, I. Volobouev, Z. Wang, A. Whitbeck

Texas Tech University, Lubbock, USA

E. Appelt, S. Greene, A. Gurrola, W. Johns, C. Maguire, A. Melo, H. Ni, K. Padeken, F. Romeo, P. Sheldon, S. Tuo, J. Velkovska

Vanderbilt University, Nashville, USA

M.W. Arenton, B. Cox, G. Cummings, J. Hakala, R. Hirosky, M. Joyce, A. Ledovskoy, A. Li, C. Neu, B. Tannenwald, E. Wolfe

University of Virginia, Charlottesville, USA

P.E. Karchin, N. Poudyal, P. Thapa

Wayne State University, Detroit, USA

K. Black, T. Bose, J. Buchanan, C. Caillol, S. Dasu, I. De Bruyn, P. Everaerts, C. Galloni, H. He, M. Herndon, A. Hervé, U. Hussain, A. Lanaro, A. Loeliger, R. Loveless, J. Madhusudanan Sreekala, A. Mallampalli, A. Mohammadi, D. Pinna, A. Savin, V. Shang, V. Sharma, W.H. Smith, D. Teague, S. Trembath-Reichert, W. Vetens

University of Wisconsin – Madison, Madison, WI, USA

[†] Deceased.

¹ Also at Vienna University of Technology, Vienna, Austria.

² Also at Institute of Basic and Applied Sciences, Faculty of Engineering, Arab Academy for Science, Technology and Maritime Transport, Alexandria, Egypt, Alexandria, Egypt.

- 3 Also at Université Libre de Bruxelles, Bruxelles, Belgium.
- 4 Also at IRFU, CEA, Université Paris-Saclay, Gif-sur-Yvette, France.
- 5 Also at Universidade Estadual de Campinas, Campinas, Brazil.
- 6 Also at Federal University of Rio Grande do Sul, Porto Alegre, Brazil.
- 7 Also at UFMS, Nova Andradina, Brazil.
- 8 Also at Nanjing Normal University Department of Physics, Nanjing, China.
- 9 Now at The University of Iowa, Iowa City, USA.
- 10 Also at University of Chinese Academy of Sciences, Beijing, China.
- 11 Also at Institute for Theoretical and Experimental Physics named by A.I. Alikhanov of NRC 'Kurchatov Institute', Moscow, Russia.
- 12 Also at Joint Institute for Nuclear Research, Dubna, Russia.
- 13 Also at Helwan University, Cairo, Egypt.
- 14 Now at Zewail City of Science and Technology, Zewail, Egypt.
- 15 Also at Ain Shams University, Cairo, Egypt.
- 16 Now at British University in Egypt, Cairo, Egypt.
- 17 Also at Purdue University, West Lafayette, USA.
- 18 Also at Université de Haute Alsace, Mulhouse, France.
- 19 Also at Erzincan Binali Yildirim University, Erzincan, Turkey.
- 20 Also at CERN, European Organization for Nuclear Research, Geneva, Switzerland.
- 21 Also at RWTH Aachen University, III. Physikalisches Institut A, Aachen, Germany.
- 22 Also at University of Hamburg, Hamburg, Germany.
- 23 Also at Department of Physics, Isfahan University of Technology, Isfahan, Iran, Isfahan, Iran.
- 24 Also at Brandenburg University of Technology, Cottbus, Germany.
- 25 Also at Skobeltsyn Institute of Nuclear Physics, Lomonosov Moscow State University, Moscow, Russia.
- 26 Also at Physics Department, Faculty of Science, Assiut University, Assiut, Egypt.
- 27 Also at Eszterhazy Karoly University, Karoly Robert Campus, Gyongyos, Hungary.
- 28 Also at Institute of Physics, University of Debrecen, Debrecen, Hungary, Debrecen, Hungary.
- 29 Also at Institute of Nuclear Research ATOMKI, Debrecen, Hungary.
- 30 Also at MTA-ELTE Lendület CMS Particle and Nuclear Physics Group, Eötvös Loránd University, Budapest, Hungary, Budapest, Hungary.
- 31 Also at Wigner Research Centre for Physics, Budapest, Hungary.
- 32 Also at IIT Bhubaneswar, Bhubaneswar, India, Bhubaneswar, India.
- 33 Also at Institute of Physics, Bhubaneswar, India.
- 34 Also at G.H.G. Khalsa College, Punjab, India.
- 35 Also at Shoolini University, Solan, India.
- 36 Also at University of Hyderabad, Hyderabad, India.
- 37 Also at University of Visva-Bharati, Santiniketan, India.
- 38 Also at Indian Institute of Technology (IIT), Mumbai, India.
- 39 Also at Deutsches Elektronen-Synchrotron, Hamburg, Germany.
- 40 Also at Sharif University of Technology, Tehran, Iran.
- 41 Also at Department of Physics, University of Science and Technology of Mazandaran, Behshahr, Iran.
- 42 Now at INFN Sezione di Bari^a, Università di Bari^b, Politecnico di Bari^c, Bari, Italy.
- 43 Also at Italian National Agency for New Technologies, Energy and Sustainable Economic Development, Bologna, Italy.
- 44 Also at Centro Siciliano di Fisica Nucleare e di Struttura Della Materia, Catania, Italy.
- 45 Also at Università di Napoli 'Federico II', NAPOLI, Italy.
- 46 Also at Riga Technical University, Riga, Latvia, Riga, Latvia.
- 47 Also at Consejo Nacional de Ciencia y Tecnología, Mexico City, Mexico.
- 48 Also at Institute for Nuclear Research, Moscow, Russia.
- 49 Now at National Research Nuclear University 'Moscow Engineering Physics Institute' (MEPhI), Moscow, Russia.
- 50 Also at St. Petersburg State Polytechnical University, St. Petersburg, Russia.
- 51 Also at University of Florida, Gainesville, USA.
- 52 Also at Imperial College, London, United Kingdom.
- 53 Also at P.N. Lebedev Physical Institute, Moscow, Russia.
- 54 Also at Moscow Institute of Physics and Technology, Moscow, Russia, Moscow, Russia.
- 55 Also at California Institute of Technology, Pasadena, USA.
- 56 Also at Budker Institute of Nuclear Physics, Novosibirsk, Russia.
- 57 Also at Faculty of Physics, University of Belgrade, Belgrade, Serbia.
- 58 Also at Trincomalee Campus, Eastern University, Sri Lanka, Nilaveli, Sri Lanka.
- 59 Also at INFN Sezione di Pavia^a, Università di Pavia^b, Pavia, Italy, Pavia, Italy.
- 60 Also at National and Kapodistrian University of Athens, Athens, Greece.
- 61 Also at Universität Zürich, Zurich, Switzerland.
- 62 Also at Ecole Polytechnique Fédérale Lausanne, Lausanne, Switzerland.
- 63 Also at Stefan Meyer Institute for Subatomic Physics, Vienna, Austria, Vienna, Austria.
- 64 Also at Laboratoire d'Annecy-le-Vieux de Physique des Particules, IN2P3-CNRS, Annecy-le-Vieux, France.
- 65 Also at Şirnak University, Şirnak, Turkey.
- 66 Also at Department of Physics, Tsinghua University, Beijing, China, Beijing, China.
- 67 Also at Near East University, Research Center of Experimental Health Science, Nicosia, Turkey.
- 68 Also at Beykent University, Istanbul, Turkey, Istanbul, Turkey.
- 69 Also at Istanbul Aydin University, Application and Research Center for Advanced Studies (App. & Res. Cent. for Advanced Studies), Istanbul, Turkey.
- 70 Also at Mersin University, Mersin, Turkey.
- 71 Also at Piri Reis University, Istanbul, Turkey.
- 72 Also at Adiyaman University, Adiyaman, Turkey.
- 73 Also at Ozyegin University, Istanbul, Turkey.

- ⁷⁴ Also at Izmir Institute of Technology, Izmir, Turkey.
- ⁷⁵ Also at Necmettin Erbakan University, Konya, Turkey.
- ⁷⁶ Also at Bozok Universitetesi Rektörlüğü, Yozgat, Turkey, Yozgat, Turkey.
- ⁷⁷ Also at Marmara University, Istanbul, Turkey.
- ⁷⁸ Also at Milli Savunma University, Istanbul, Turkey.
- ⁷⁹ Also at Kafkas University, Kars, Turkey.
- ⁸⁰ Also at Istanbul Bilgi University, Istanbul, Turkey.
- ⁸¹ Also at Hacettepe University, Ankara, Turkey.
- ⁸² Also at Vrije Universiteit Brussel, Brussel, Belgium.
- ⁸³ Also at School of Physics and Astronomy, University of Southampton, Southampton, United Kingdom.
- ⁸⁴ Also at IPPP Durham University, Durham, United Kingdom.
- ⁸⁵ Also at Monash University, Faculty of Science, Clayton, Australia.
- ⁸⁶ Also at Bethel University, St. Paul, Minneapolis, USA, St. Paul, USA.
- ⁸⁷ Also at Karamanoğlu Mehmetbey University, Karaman, Turkey.
- ⁸⁸ Also at Bingol University, Bingol, Turkey.
- ⁸⁹ Also at Georgian Technical University, Tbilisi, Georgia.
- ⁹⁰ Also at Sinop University, Sinop, Turkey.
- ⁹¹ Also at Mimar Sinan University, Istanbul, Istanbul, Turkey.
- ⁹² Also at Erciyes University, KAYSERI, Turkey.
- ⁹³ Also at Texas A&M University at Qatar, Doha, Qatar.
- ⁹⁴ Also at Kyungpook National University, Daegu, Korea, Daegu, Republic of Korea.